ISOTHERMAL TRANSFORMATIONS IN DUCTILE IRON

A THESIS

Presented to

The Faculty of Graduate Division

by

Nirmal Kumar Datta

In Partial Fulfillment

of the Requirements for the Degree

Doctor of Philosophy

in the School of Chemical Engineering

Georgia Institute of Technology

December, 1973

ISOTHERMAL TRANSFORMATIONS IN DUCTILE IRON

Approved:

Chairman

Date Approved by Chairman Dec. 20 - 1973

ACKNOWLEDGEMENT

The author wishes to express his deep appreciation to his thesis advisor, Dr. Niels N. Engel, for suggesting the problem and for his inspiring guidance, sustained encouragement and stimulating discussions.

The author is also greatly indebted to Drs. Stephen Spooner and Edgar A. Starke, Jr., for having taken time to review this work. Their interest and constructive criticism is highly appreciated.

It gives the author great pleasure to thank Drs. E. E. Underwood and R. F. Hochman for having many helpful discussions while this work was in progress.

The author would like to express his gratitude and sincere thanks to his fellow graduate students, Messrs. John G. Rinker, Roberto Piccinini, Henry G. Paris, G. Rubino, A. H. Roy, R. Kumar, K. H. Chien, K. Ansah and others for providing experimental assistance in this work.

The author is also greatly indebted to the American Cast Iron Pipe Company, Birmingham, Alabama, for the supply of raw material and the chemical analyses of the specimens.

The financial support of this research provided by the Ductile Iron Society is gratefully acknowledged.

TABLE OF CONTENTS

TABLE OF CONTENTS (Continued)

LIST OF TABLES

LIST OF FIGURES

LIST OF FIGURES (Continued)

LIST OF FIGURES (Continued)

SUMMARY

Isothermal transformation diagrams for decomposition of cementite in ductile iron containing varying amounts of Si, Mn, Cu and Cr have been made by metallographic technique. The specific points of investigation were the determination of optimum additions of ferrosilicon (FeSi), quantitative metallography determination of nucleation and growth of graphite during isothermal graphitization, and electron microprobe analysis of alloy element segregation behavior in samples quenched during the solidification process which relates to the mechanism of nodular graphite formation in ductile iron.

A batch of about 1350 gms of base iron was melted and inoculated by pouring the molten iron over SiMg alloy. Post-inoculation with ferrosilicon was performed by pouring the melt on to the 1/4 inch size ferrosilicon (FeSi) particles kept at the bottom of a red hot crucible. Initially a step bar was cast in a sand mold and this was followed by pouring the melt into a series of graphite molds placed in seven constant temperature holding furnaces. Graphite molds with the specimens were then taken out of the furnace at desired time intervals and quenched in water to freeze the transformation. The isothermally treated samples were ground and polished in several transverse and longitudinal directions for examination under optical microscope. Some samples were used for microprobe analyses.

Results of the present research showed that the isothermal growth of graphite was primarily controlled by the solution of

cementite at an earlier stage and re-solution of smaller nodules at the later stage. The T-T-T curve for decomposition of cementite was shifted to shorter times with higher addition of Si. However, this effect is more pronounced when Si was added after Mg treatment. Furthermore, the amount of residual carbide in thin sections was considerably reduced when FeSi was added after Mg inoculation. Microanalytical results indicated that the Si and Cu segregate in the austenite and Mn segregates in the carbide during the process of solidification. It also showed that the growth of nodular graphite does take place directly in contact with the liquid at an earlier stage of solidification.

CHAPTER I

INTRODUCTION

Because of growing demand for materials with high strength, toughness and good ductility, the discovery of ductile iron is a remarkable breakthrough in cast iron metallurgy. This material, with spectacularly better engineering properties than other varieties of cast iron and steel, produces a direct measurable benefit to the consumer.

At present ductile iron is one of the major foundry products (1), exceeding in tonnage and value both malleable iron and steel. The demand for ductile iron castings can be increased further if the properties of this material can be improved by suitable casting and heat-treating techniques. In order to improve tensile strength, ductility, impact strength, fatigue, etc., it is essential to investigate several key factors such as the mechanism of nucleation and growth of spheroidal graphite, kinetics of graphitization, correlation between cooling velocity, and matrix structure of the castings and the influence of different alloying elements on the aforementioned factors.

The kinetics of isothermal graphitization, although very important for industrial grade ductile iron, has been little studied so far. However, in the past several years Russian investigators (2, 3, 4, 5) have attempted to construct the time-temperature-transformation curves for isothermal structure development in cast iron.

However, those curves do not reveal any information regarding the influence of alloying elements, post-inoculation and other variables which are frequently encountered in actual foundry practice. Thus there is a need for an extensive investigation of the nucleation and growth of graphite and the time-temperature-transformation curve of the dissociation of cementite in ductile iron.

Therefore the present study has primarily concentrated on the nucleation and growth of graphite and dissociation of cementite during isothermal transformation. The main effort was directed to study the influence of the alloying elements; Si, Mn, Cu and Cr on the speed of isothermal graphitization and the distribution of these alloying elements at different stages of graphitization. Thereby an attempt has been made to establish the possible mechanism of nucleation and growth of spheroidal graphite in the process of solidification.

The influence of post-inoculation with FeSi has also been investigated in this work. In addition, a correlation between cooling velocity and the matrix structure has been established by superimposing the cooling curve on the T-T-T curve.

Furthermore, quantitative measurements of ferrite, pearlite and carbide have been made and plotted against the casting section thickness. Thus it appears possible to predict the microconstituents in the ductile iron solidified under different cooling conditions.

CHAPTER II

REVIEW OF LITERATURE

Formation of Nodular Graphite from Solid or Liquid State

Since the discovery of ductile iron by Gagnebin, Millis and Morrough (5,6,7,8), large quantities of this iron is now produced throughout the world. The mechanism of solidification of ductile iron is, however, a subject of much controversy and speculation.

In normal grey cast iron, the graphite is in the form of flakes of various sizes according to casting section size, composition and melting procedure. These graphite flakes interrupt the continuity of the matrix and by acting as stress raisers, reduce the strength properties of the aggregate. In ductile iron, the graphite precipitates in spheroidal shape and, in contrast to flake graphite in grey cast iron, does not significantly interrupt the continuity of the metallic matrix. This transition from flake to spheroidal graphite radically changes the physical properties and results in a high tensile ductile iron. The vast amount of literature available today reveals diversified opinions and contradictory conclusions as regards to the nucleation and growth of spheroidal graphite in cast iron.

Several theories have been suggested on the formation of nodular graphite in cast iron. One group (8,9) suggests that nodular graphite forms indirectly by breakdown of cementite in solid state, with graphite growing inside an austenite shell. It is clear that

this theory predicts that the nucleation of graphite occurs exclusively in solid state and does not take place directly in contact with the liquid.

According to a recent theory (10,11) however, the spheroidal graphite nucleates directly from the melt in normal circumstances. Owing to the low density of carbon compared to that of the liquid iron, the graphite spheroid will show a tendency to float on the surface of the melt. Floatation of graphite nodules in heavy section ductile iron castings has been reported by many investigators (12,13,14,15). Separation of graphite nodules by centrifuging (16,17) ductile iron melt also clearly establishes the fact that the spheroids arise from the liquid state. Furthermore, the work of Schiel et al. (18,19) also supports the idea that nodules form directly in contact with the liquid.

Figure 1 represents schematically the three alternative hypotheses for the solidification of ductile iron. Figure 1 (a) is the most widely accepted of these theories and has been suggested by several investigators from ductile iron samples quenched during the solidification process (20,21,22,23,24,25). According to this theory, small graphite spheroids form initially from the liquid and become rapidly encapsulated by a rim of solid austenite. Concurrent growth of the graphite and austenite then continues by diffusion of carbon from the liquid to the graphite nodule via the austenite envelope. This process will continue until the graphite eutectic cells impinge and solidification is completed. When the clustering of eutectic cells takes place, the

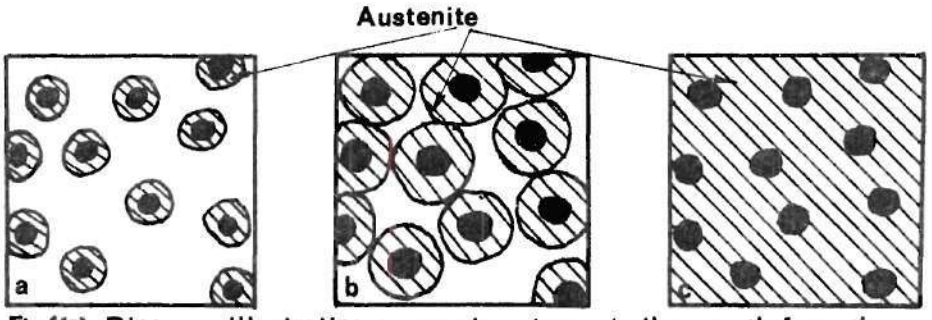

Fig 1(a). Diagram illustrating successive stages in the growth from the liquid of the nodular graphite eutectic

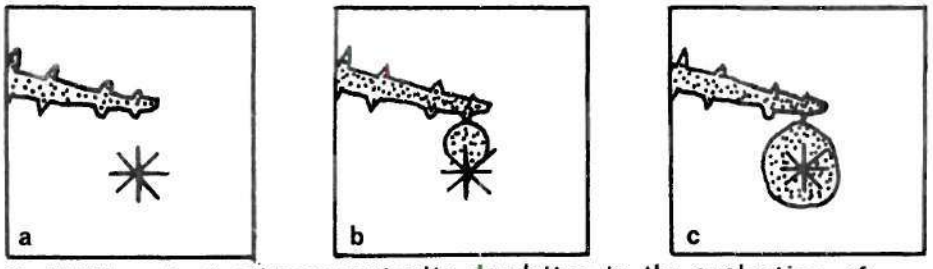

Fig 1(b). The role of primary austenite dendrites in the nucleation of carbon depleted liquid

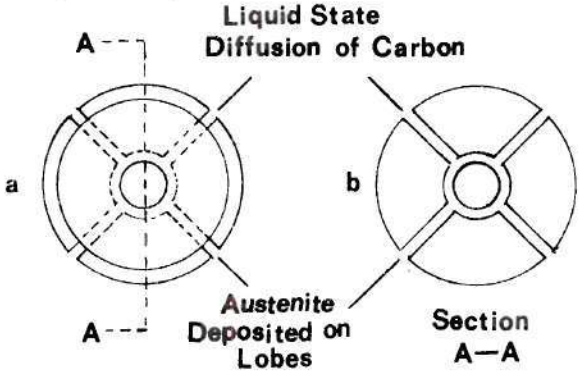

Fig 1(c). Exaggerated model for growth of nodular cast iron

Figure 1. Schematic Arrangement of Three Alternative Hypotheses for the Solidification of Nodular Iron (25).

solidification is completed by the impingement of the clusters containing several nodules (26).

Figure 1 (b) explains schematically the ductile iron solidification theory proposed by Oldfield, Geering and Tiller (27). These authors suggested that graphite nodules first form from the liquid as graphite filament arrays. These graphite crystals reject iron into the liquid surrounding them, building up a layer of carbon-depleted liquid which is constitutionally supercooled. This layer subsequently solidifies as an austenite envelope encapsulating the graphite crystals.

In the second stage, the nucleation and solidification of austenite considerably slows down the nodular growth (28,29). During this stage, the austenite grows in contact with the melt. Solidification is mostly completed at this stage, but the graphite nodule may grow little further in solid state either by diffusion of carbon through the austenite shell or by transformation of austenite to ferrite during cooling. This results in a deposition of carbon on the existing graphite spheroids.

In the third stage, the austenite shells themselves exhibit a considerable growth. This growth is accompanied by the formation of a carbon rich boundary layer in the melt. This high carbon layer will finally deposit carbon in the last to solidify austenitic grain boundaries. This may result in a non-spheroidal type of graphite in the final structures as is often found in case of heavy section ductile iron castings.

This theory explains very well different stages of nodular iron solidification. The only drawback of this theory, as pointed out by

Jolley (25), is the assumption of 'filament arrays' of graphite which has not been reported so far by any investigator who studied the solidification of ductile iron by quenching techniques.

Figure 1 (c) illustrates a refinement to the original theory of eutectic growth which has been proposed by Jolly (25,30). This author found the presence of carbide filaments connecting graphite nodules to the quenched liquid in the specimen of nodular iron quenched during solidification. Based on this observation, Jolly proposed a mechanism which is illustrated in Figure 1 (c). This theory suggests that the liquid diffusion of carbon takes place along thin channels to the graphite nodules, thus leaving a carbon depleted zone at the periphery of the austenite lobes surrounding the nodules. During the solidification process the growth of the graphite is accommodated by the outward sliding of these austenite lobes. The liquid diffusion of carbon in this theory was supported by the fact that the carbon diffusion in liquid iron is 20 times faster than in solid austenite at the same temperature (31).

Solidification of Ductile Iron

While the solidification of grey iron is well explained and widely accepted, the eutectic solidification of ductile iron is still a subject of considerable research by many investigators.

In grey iron, the eutectic solidification (32) involves the nucleation and growth of graphite and austenite eutectic cells in the temperature range 1148 to 1098°C. The graphite flake grows with its tip in contact with the molten iron.

By contrast in ductile iron, it is a matter of considerable discussion whether the graphite spheroids grow directly in contact with the melt or these spheroids are protected by an envelope of austenite shell.

According to H. Morrough (20), the sequence of solidification can be presented as follows:

1) Hypo-eutectic irons - Primary austenite dendrites form directly from the liquid. Graphite nodules appear either just before or at the beginning of the eutectic solidification.

2) Hyper-eutectic irons - Graphite spheroids form directly from the melt,until at the eutectic transformation, austenite envelopes develop round the nodules and nodule growth takes place by diffusion of carbon from the liquid through the austenite to the nodule.

Dunphy and Pellini (33,34) studied the solidification of nodular iron by quenching methods. These authors concluded that the hypo-eutectic nodular iron solidify in three steps. These are: (1) formation of primary austenite dendrites, (2) nucleation of graphite nodules near the dendrites or on the interstices between dendrite arms, and (3) solidification of the remaining liquid as an austenite carbide complex that decomposes with additional cooling to austenite and graphite. According to these authors, the decomposition of carbide does not change the number of nodules but enhances the size of the existing nodules.

Solidification studies by Loper, Heine and several other investigators (22,24), however, indicated that the nodule number decreased at lower quenching temperatures. While Dunphy and Pelleni reported

that the number of nodules is independent of the quenching temperatures.

Loper and Heine proposed that the graphite spheroids are nucleated at about 1343 to 1371°C as shown in Figure 2. These graphite nuclei grow into spheroids which are encapsulated by austenite shells. Thus the spheroids do not come in contact with the liquid and the spheroidal shape is well maintained. On the other hand, if the austenite shell is absent, the graphite grows in flake shape having its tip in contact with the liquid.

In contrast, the growth of the spheroidal graphite takes place by diffusion of carbon through the austenite shell to the graphite and diffusion of iron and silicon away from the graphite to provide room for its growth. The growth of a graphite shperoid is accompanied by a corresponding thickening of austenite shell. Since only austenite is in contact with the liquid, the solidification takes place in a neo-eutectic mechanism (35). The neo-eutectic growth of graphite is a special case of degenerate eutectic formation because graphite spheroids can grow even though the spheroids are isolated from the eutectic liquid by an austenite shell. Carbon can diffuse interstitially through the austenite lattice. Wieser, Bates and Wallace (36) point out that this theory is not in agreement with the phase diagram.

Influence of Post-Inoculation

One of the essential requirements in the production of high quality ductile iron is the nucleation of an adequate number of graphite spheroids in order to avoid residual carbides and non-spheroidal graphite in the as-cast structure. The most significant factors (37,38)

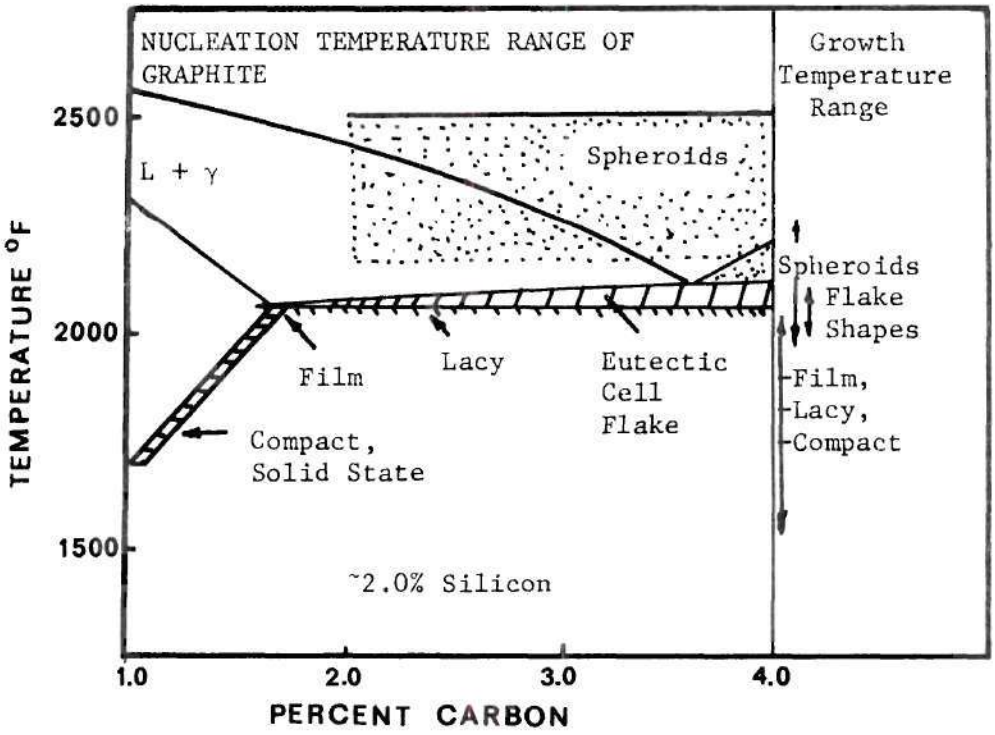

Figure 2. Fe-Si-C Phase Diagram Section Showing Schematically the Nucleation and Growth Temperature Range for Various Graphite Types Including Spheroids (36).

which control the nodule count in the ductile iron structures are: (1) carbon equivalent or metal chemistry (2) section size of the casting (3) magnesium treatment and post-inoculation and (4) process cycle variations. If any of these factors is not properly controlled during the production process, mechanical properties of ductile iron are severely reduced due to the presence of residual carbide or undesirable graphite shapes in the structure.

Generally, the additions to the ductile iron melt can be broadly divided into two categories (37):

(1) Those additions which cause an increase in the amount of nodular graphite

(2) Those additions made to suppress graphite nucleation other than nodular graphite in the neo-eutectic solidification range.

Magnesium falls into both the categories. In the production process,however, FeSi is the most widely used material to increase the nodule count in the as cast structure. Normally, FeSi is added after magnesium treatment. Addition of FeSi prior to magnesium treatment or simultaneously with magnesium has been found to be ineffective (39).

Post-inoculation with FeSi changes the solidification behavior and structure of cast iron. Owing to the inoculation treatment, the number of graphite nucleation centers is greatly increased and thereby the undercooling of the melt is reduced. However, as the holding time in the liquid state is prolonged, the undercooling increases again. Therefore, the influence of post-inoculation is time-dependent and in order to avoid the reduced effectiveness of FeSi inoculant, the melt should be poured into the mold as quickly as possible after inoculation.

Kinetics of Nucleation During Post-Inoculation

Several hypotheses (36,40,41,42) have been advanced on the heterogeneous nucleation of graphite in ductile and grey iron, and it appears that the heterogenieties effective for the nucleation or solidification of flake graphite are effective for spheroidal graphite as well. Therefore the nucleation of nodular graphite could be effected by salt-like carbides such as calcium carbide, barium carbide, graphite from the decomposition of silicon carbide, undissolved graphite particles in the melt and reaction products of the nodularizing additions.

One of the classic theories, presented by Lux (43,44) is based on the heterogeneous nucleation on substrates of salt-like carbides introduced with the addition of nodularizers and especially with post-inoculants. According to this author, the formation of the salt-like carbides can occur only under the non-equilibrium conditions encountered during the inoculation process. Under equilibrium conditions, however, the salt-like carbides become unstable and this results in a lowering of effective crystallization centers with longer holding time of the melt.

The kinetics of nucleation as presented by Lux can be stated as follows (43): the solid Fe-Si inoculant bearing the reactive metals is added as small grains. These grains dissolve and form in the melt localized regions of higher silicon concentration, and thus localized hyper-eutectic zones are formed surrounding the nodules. On the other hand the metallic impurities in the inoculants will remain in metallic form in these zones after dissolution of the iron and silicon.

Because of their lower solubility (45) in liquid iron, finely dispersed particles are formed within the melt. In the case of reactive metals like calcium, metallic droplets are formed and they remain suspended in the melt. At the melt-droplet interface, an oxygen and sulfur free region facilitates the formation of metallic carbides.* These carbides are not stable under equilibrium conditions as can be seen from the free energy of formation (Figure 3), but they react to form more stable oxides and sulfides. Owing to this chemical reaction the number of effective crystallization centers will decrease with time and thus the fading of inoculation effect is well explained.

Graphitization in Solid State

Kinetics of graphitization in the solid state presents an entirely different situation from that in the liquid state. The sequences of graphitization (46) in liquid state can be

$$(\text{Carbon})_{\text{liquid iron}} \rightarrow \text{Graphite} \qquad (1)$$

This proeutectic reaction accounts for the precipitation of graphite with decreasing temperature. At the eutectic temperature, the reaction takes place as

$$\text{Liquid iron} \rightarrow \text{Austenite} + \text{Graphite} \qquad (2)$$

In contrast to the reactions (1) and (2), the graphitizing reaction in solid state can be written as

*Which become more effective due to precipitation of carbon from hyper-eutectic silicon rich zone.

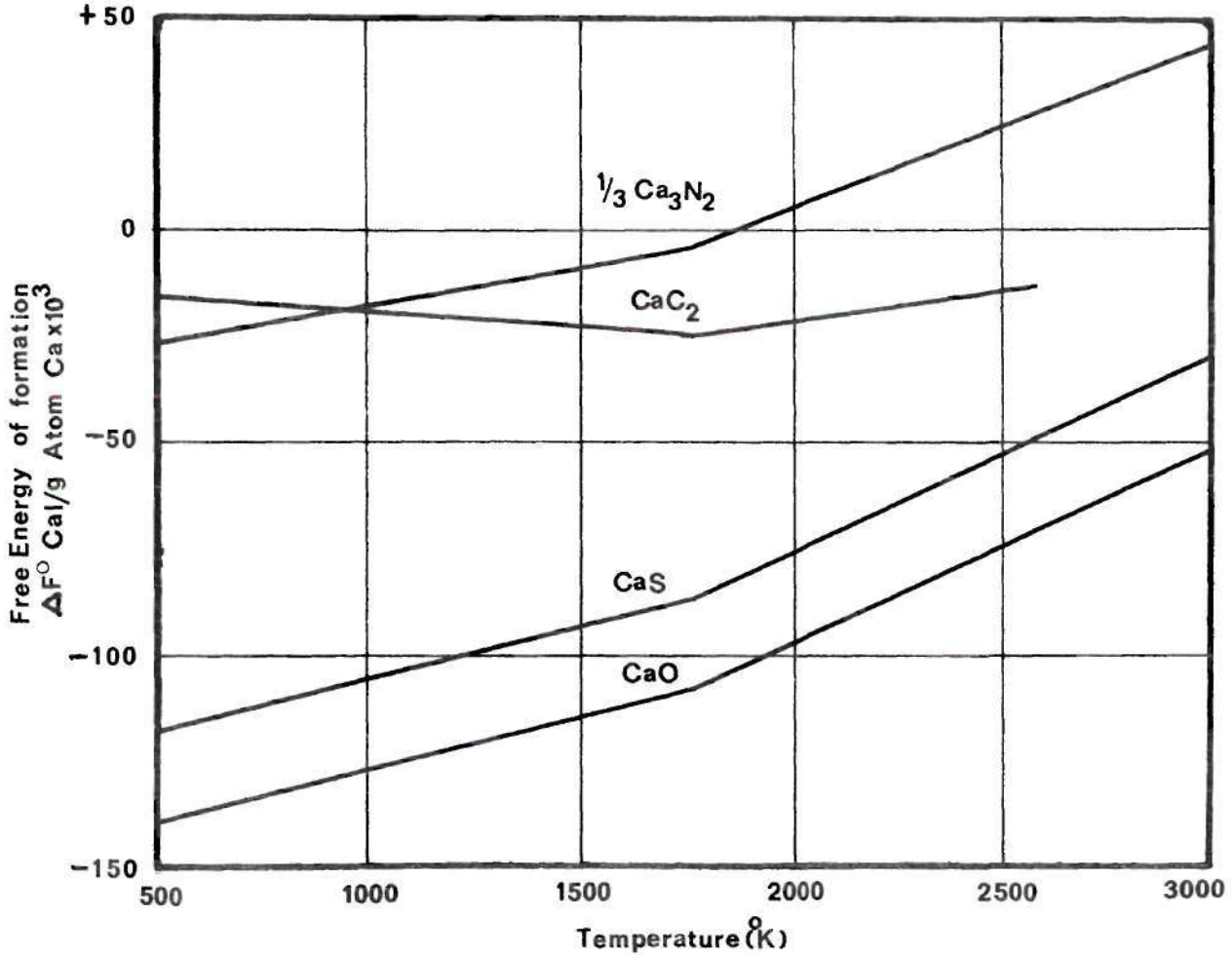

Figure 3. Free Energy of Formation of Some Calcium Compounds(43).

$$\text{Cementite} \rightarrow \text{Austenite} + \text{Graphite} \qquad (3)$$

This reaction represents the decomposition of massive cementite from the white iron structure.

In addition, the precipitation of graphite along the $A_{graphite}$ line (46) is presented as

$$(\text{Carbon})_{austenite} \rightarrow \text{Graphite}.$$

The graphite so rejected from austenite deposits on the existing graphite.

Since the isothermal transformation studies in the present work has been done above the eutectoid temperature, the graphitizing reaction below the eutectoid temperature will not be elaborated here.

Kinetics of graphitization in commercial white iron has a great technical significance, since it reveals important information about the optimum malleablizing time, graphite morphology, matrix structure and hence the mechanical properties. As a result, many investigators attempted to establish a model of graphitization kinetics in commercial white iron.

Johnson and Mehl (47), Austin and Ricketts (48) and Burke and Owen (49) developed several empirical equations which account for the kinetics of the first stage graphitization in white iron. However, these models cannot be directly applied in the present study of isothermal transformation in ductile iron. In the present work, the molten iron is not quenched to the room temperature to get white iron which consists of cementite and pearlite and no graphite. Instead, the ductile

iron melt was quenched to the isothermal reaction temperature and then held for different time intervals for the first stage graphitization. In the Johnson-Mehl, Burke-Owen and several other models it is presumed that the structure does not have any graphite nodule at the time t=0, whereas in the present work graphite nodules are formed while quenching to the isothermal temperature. Consequently, the graphitization rate is greatly accelerated at the beginning of transformation. At the later stage, however, the kinetics of graphitization may be somewhat similar to that of white iron, therefore some of the previous studies concerning the first stage graphitization in white iron will be reviewed here.

Nucleation of Graphite

First stage graphitization in white iron occurs by a process of nucleation and diffusional growth (50). Heterogeneous nucleation of graphite takes place at the interfaces between austenite and eutectic cementite or at the surface of inclusions (49)(51). According to Taube (52), Gill and Epplesheimer (53), the possible nucleation sites are located at the interface between austenite and small carbide particles remaining in the austenite. Walker, Kondic (54) and several other authors found from the metallographic examination that the nucleation sites are always associated with the massive eutectic cementite.

Graphitization (55) proceeds by dissolution of carbide in the austenite and diffusion of carbon through the austenite to the graphite nuclei. The number of nuclei varies with the composition and thermal history. In general, graphitizing elements increase the number of nodules while the carbide stabilizers reduce it. Refinement of eutec-

tic structure also enhances the nodule number by increasing the interfacial area available for nucleation.

Growth of Graphite

Growth of graphite during isothermal graphitization involves the following processes (50):

a) dissolution of cementite

b) diffusion of carbon through the austenite

c) precipitation of carbon atoms onto the graphite lattice

d) removal of iron, silicon and other solute atoms from the moving interface.

These processes are interdependent. If the precipitation of carbon is the slowest step, then a constant carbon potential is maintained in the austenite so long as any carbide remain undissolved. According to Burke (56) the rate of growth would be constant for most of the reaction time because of the homogenity of the carbon content in the austenite.

Burke and Swindelles (50) reported in their paper that the rate of solution of cementite and the rate of carbon diffusion were the two processes which could control the growth of graphite. Results of Binchenall and Mead (57) and Brown and Hawkes (46) show that the growth of graphite is diffusion controlled. To the contrary, however, the work of Burke and Owen (49) and Wilcock (58) on high purity iron-carbon-silicon alloys shows that the growth rate is controlled by the solution of cementite in austenite.

Ashton and Newall (48) studied the first stage graphitization of silicon bearing white cast irons. These authors concluded from their

results that up to about 40% transformation, growth of graphite is controlled by diffusion of iron and silicon atoms away from the graphite particles. Subsequently, growth is controlled by the rate of solution of cementite.

Redistribution of Graphite Nodule

It has been reported by McMillan (59), Brown and Hawkes (46), Burke and Owen (49) that the number of nodules decreases when the isothermal graphitization time is longer than that necessary to remove all the carbides in the structure. According to Burke and Owen, nodules with a radius less than some critical value redissolve, and carbon diffuses through the austenite and deposit upon larger growing nodules. This mechanism is further supported by Owen and Wilcock in their studies of first stage graphitization in Fe-C-Si alloys.

Owen and Wilcock (58) considered two possible cases of the graphite growth. The carbon level in the austenite may start to fall as soon as graphitization starts, in which case resolution of the smallest nodules takes place continuously throughout the reaction and simultaneously with the growth of the larger nodules. Alternatively, the rates of solution of cementite and diffusion of carbon atoms into the austenite may be sufficient to maintain a constant carbon level for a certain length of time.

The re-solution of graphite will not occur until a time is reached when the carbon replenishment from the cementite fails to keep pace with the depletion resulting from the graphite growth.

At the end of the graphitization reaction, when all the cementite becomes dissolved, the austenite will be just saturated in the

vicinity of the smallest existing nodules. Since the interfacial energy per unit volume is greater for smaller nodule than for larger, the energy of the system as a whole would be reduced by the growth of the larger nodules at the expense of the smaller nodules.

Results of the present work on the isothermal growth of graphite in ductile iron, also show that the number of graphite nodules decreases with increasing holding time. The details of this mechanism will be discussed in Chapters IV and V.

Influence of Alloying Elements

The common alloying elements are Si, Mn and Cu. Occasionally a strong carbide stabilizer like Cr causes residual carbide in the ductile iron structure. Therefore, the influence of Cr on the isothermal graphitization is also included in this work.

Previous investigators (60,61,62) have attempted to study the effects of alloying elements on the first stage graphitization of white iron. However, not much research has been done on the influence of alloying elements in the isothermal graphitization of ductile iron. In particular, the effect of alloying elements on the T-T-T curve for decomposition of cementite has been first studied in this thesis. Therefore direct information concerning the influence of alloying elements on the graphitizing behavior of ductile iron is not available from the published literature. However, the general effect of alloying elements on the stability of carbide and the influence of alloying elements on the nucleation of graphite will be discussed in this chapter.

Silicon is a strong graphitizer and as such it accelerates the rate of decomposition of cementite in cast iron. Oldfield (63) reported that the chilling tendency of an iron can be reduced by increasing its silicon content. This is mainly due to the increasing difference between the graphite and ledeburite eutectic temperatures with increasing silicon contents (Figure 4).

The nucleation of graphite nodules can be markedly increased by post-inoculation with FeSi, thereby the likelihood of carbide formation in the as cast structure is greatly minimized. The larger number of graphite nuclei lower the distance between the carbide and graphite particles and thereby accelerate the decomposition of cementite. The nucleation rate (64), however, decreases when the metal is held for a longer time in liquid state either in the furnace or in the ladle.

It is also interesting to note that the nucleation rate achieved by post-inoculation with FeSi is much stronger than that obtained by equivalent amount of silicon addition during melting of the charge (39).

A recent study by Shaw et al. (65) reveals that there is an optimum percentage of FeSi which yields an optimum increase in the number of nodules by post-inoculation. Addition of more FeSi does not increase the number of nuclei further and is therefore not advantageous.

Manganese normally reacts with sulfur to form manganese sulfide and tends to separate out from the melt by flotation. To be effective, the percentage of manganese required to neutralize the sulfur in the melt is equal to 1.7 x the sulfur content. The reaction (66) between manganese and sulfur is, however, reversible and consequently in order to ensure that all the sulfur is neutralized by manganese, the required

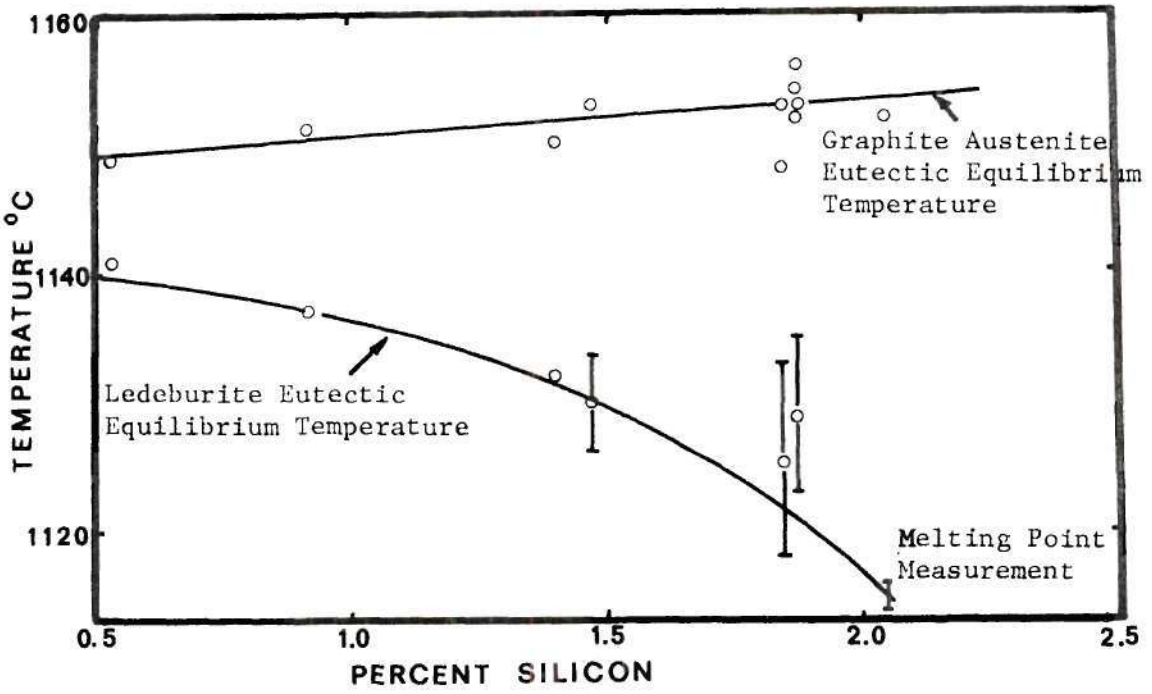

Figure 4. Effect of Silicon on the Two Eutectic Equilibria(63).

manganese content should be equal to 1.7 x the sulfur content + 0.3, or at least 5 times the S content.

In ductile iron, the amount of manganese in excess of that reacting with sulfur acts as a carbide stabilizer and promoter (39). Manganese also has a tendency to segregate in the last portion of the liquid to solidify and thereby manganese-rich carbides are formed in the ledeburite.

The manganese content (39) in 1/4 inch ductile iron casting should be approximately 0.2 percent and in lighter sections, a completely manganese-free composition is recommended.

Since manganese acts as a carbide stabilizer, it inhibits the nucleation of graphite in ductile iron.

In the past, it was thought that copper has an adverse effect on the graphite shape in ductile iron. However, investigation by Morrough (67) in the magnesium-treated irons showed that copper is not itself a subversive element. In the absence of titanium, lead, antimony, bismuth, aluminum, tin and arsenic, up to 3.0 per cent of copper can be tolerated without any adverse effect (68) but above 3.0 per cent there is a tendency to cause flake graphite.

Copper is not a carbide forming element and it is expected that only very little copper can be dissolved in cementite. According to Albert DeSy (69) copper refines the ledeburite and cementite. This is attributed to the influence of copper on the diffusion rate of carbon. A decreased growth rate of carbon rich crystals refines the cementite size in the ledeburite structure.

Copper is a mild graphitizer. According to the literature (69),

the graphitizing effect of copper is estimated between 1/3 and 1/5 that of silicon. However, according to Albert DeSy, it should be close to 1/5 that of silicon.

Thus copper refines the ledeburite and has practically no influence on graphite nodule count and size.

Chromium acts as a powerful carbide stabilizer and thereby it reduces the formation of free graphite. If the graphitizing power of silicon is taken as unity, then the graphitizing power of chromium is -1 (68) to -1.2 (66). The carbon content of the eutectic is reduced by about 0.5 per cent for each 1.0 per cent addition of Cr. At about 3.0 per cent chromium, the formation of free graphite is suppressed and a white iron structure results. In ductile iron, the upper limit of chromium is 0.03 per cent (39).

Oldfield (70) has shown that increasing chromium content raises the ledeburite eutectic temperature and thereby reduces the temperature difference between the metastable eutectic and the graphite eutectic. Consequently the carbide stability of the iron is greatly increased.

Investigation of the Distribution of Alloying Elements in the Ductile Iron Structure by Electron Microprobe Analysis

Recently the electron microprobe study of the segregation of various alloying elements in ductile iron has been undertaken by several investigators (29,30,71,72). The nature of distribution of the solute atoms led to the understanding of the many currently held hypotheses of the solidification of ductile iron. Many key factors such as the mechanism of nucleation and the growth of graphite, the stability of carbides and degeneration of spheroids to vermicular or exploded forms

can be logically explained from the segregation pattern of the alloying elements in the ductile iron structure.

A. P. Von Rosentiel and co-workers (72) investigated the nature of the graphite nuclei by x-ray microanalysis. According to the microprobe analysis by these authors, it was found that the elements Si and Mg occured in a fixed ratio of concentration in the center of the graphite nodule. This indicated that the nucleating agent consisted of a magnesium-silicon bearing compound.

In order to verify the identity of the nucleating agent, further investigations were carried out by taking electron diffraction pattern of the graphite nodules separated from the fractured specimen and from the diffraction pattern, the authors identified the magnesium-silicon compound as $3MgO$, $2SiO_2$, $2H_2O$.

Albert DeSy (73) also studied the core of the spheroidal graphite by spectrographic analysis of the graphite separated from the metallic matrix. It was found that the graphite contained proportionally more Mg than the average content of the iron from which the graphite nodules were separated. Based on this result the author concluded that the graphite spherulite results from the decomposition of a complex magnesium-silicon-carbide. Among all the existing theories of nodular graphite formation in ductile iron, the most commonly accepted theory states that at some temperature small graphite nodules form, initially from the liquid (20,21,22,23,24) and become surrounded by an envelope of austenite. The graphite and austenite then grow together by solid state diffusion of carbon from the liquid to the graphite nodule via the austenite shell. This process continues until the nodular graphite

eutectic cells impinge and solidification is complete. With increasing growth of the austenite shell the diffusion distance of carbon atoms will increase and the solidification is delayed.

This mechanism differs from the normal theories of eutectic solidification. According to the previous theory only one-phase austenite grows in contact with the liquid and a substantial amount of solid state diffusion has to take place for the solidification of nodular iron. Since the diffusion of carbon in liquid iron is 20 times higher than the diffusion in solid austenite at the same temperature (31) it is believed that the cast iron would solidify by liquid diffusion of carbon.

In order to resolve the differences between the nodular graphite formation models, Riding and Gruzleske (29) performed electron probe analyses on ductile iron containing various alloy additions. According to these authors the expected concentration profiles for two possible modes of solidification of ductile iron is shown in Figure 5. If no austenite shell is formed, solute would segregate at the graphite/melt interphase as in curve (a) of Figure 5. However, if an austenite envelope is present during freezing, solute concentration will occur at the austenite/liquid interface as shown in curve (b).

The electron microanalyses of Riding et al. showed no evidence of an austenite shell and consequently these authors concluded that such a shell is not a requisite for spheroid formation.

Similar type of analysis has been done by Jolley (30) who found the presence of austenite shell in specimens quenched at successive

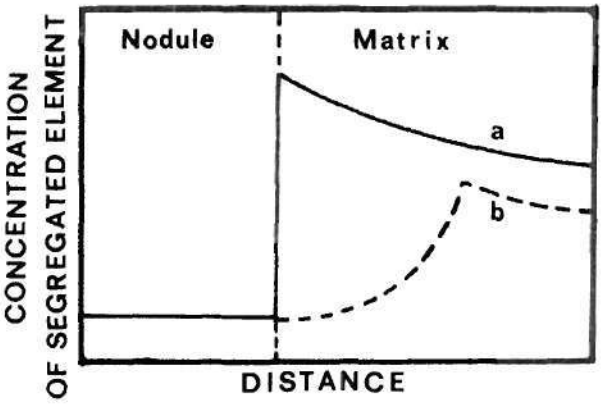

Figure 5. Schematic Segregation Profiles for Elements with Distribution Coefficients Less Than Unity. (a) No Austenite Shell is Present, (b) An Austenite Shell is Present (29).

time during eutectic arrest. He postulates that the growth of spheroidal graphite takes place by liquid diffusion of carbon along the thin channels within the austenite shell.

The work of Jolley differs from that of Riding and Gruleski (29) who found no evidence of austenite shell. The possible reason might be that the samples which indicated austenite rim were held longer time after the start of the eutectic arrest, whereas the samples which indicated no austenite shell resided for shorter time at the eutectic temperature.

CHAPTER III

EXPERIMENTAL PROCEDURE

Melting and Processing

Ductile iron batches were melted in a 15 KW Lepel high frequency furnace, using a fireclay crucible. The base iron was produced in a basic cupola by American Cast Iron Pipe Company, Birmingham, Alabama. The analysis of the iron is given in Table I.

A batch of about 1350 gms of base iron was melted and inoculated by pouring the molten iron over the SiMg alloy containing 9.0 per cent Mg. About 68 grams of SiMg alloy was used for 1350 grams of base iron in order to get a Mg content of 0.04 to 0.06 per cent in solution. The temperature of the melt was approximately 1395°C as measured by an optical pyrometer. The composition of different heats were varied by adding FeSi, FeMn, FeCr and Cu before magnesium treatment. Post-inoculation with FeSi (85% Si) was performed by pouring the melt onto the 1/4 inch size FeSi particles kept at the bottom of a red hot crucible.

After inoculating the melt with SiMg alloy, the dross was skimmed off from the surface and the molten iron was immediately poured into three different types of mold. Initially a chill sample was cast in a copper block for chemical analysis. This was followed by casting a step bar in a sand mold and the remaining metal was poured into

Table 1. Chemical Analyses of Research Materials

Base Iron

C	3.95	S	0.022	Cr	0.038	Ni	0.02
Si	1.74	P	0.034	Mo	0.02	Cu	0.051
Mn	0.96	Mg	0.01	V	0.034	Sn	0.004
Ti	0.027	Pb	0.001	Al	0.01		

Experimental Alloys

Alloy	C	Si	Mn	Cu	Cr	S	P	Mg
GT-41	3.84	2.13	1.67	0.058	0.046	0.035	0.02	0.032
GT-42	3.65	2.53	2.05	0.054	0.051	0.026	0.024	0.048
GT-44	3.64	3.03	0.85	0.055	0.38	0.026	0.017	0.07
GT-49	3.60	2.56	0.83	2.13	0.041	0.016	0.017	0.085
GT-50	3.70	2.06	0.92	0.046	0.043	0.031	0.023	0.045
GT-51	3.70	1.95	0.84	0.044	0.042	0.030	0.017	0.03
GT-52	3.48	4.10	0.74	0.044	0.047	0.025	0.022	0.06
GT-54	3.69	2.30	0.89	0.04	0.044	0.026	0.025	0.041
*GT-58	3.70	2.37	0.69	0.11	0.073	0.033	0.020	0.057
*GT-59	3.85	2.25	0.69	0.13	0.07	0.029	0.017	0.034
*GT-60	3.42	2.80	0.73	0.12	0.06	0.033	0.014	0.064
GT-61	3.63	2.31	0.80	1.07	0.039	0.022	0.03	0.08
*GT-62	3.67	2.71	0.68	0.10	0.045	0.021	0.013	0.042
*GT-63	3.56	2.33	0.68	0.04	0.071	0.027	0.019	0.056
GT-64	3.67	3.02	0.85	0.06	0.045	0.019	0.020	0.049

* Post-Inoculated with FeSi.

several graphite molds which were placed in seven constant temperature holding furnaces.

Design of Holding Furnace, Graphite Mold and Pouring Basin

Holding furnaces of 6x8x9 inches inside were made out of 3 inches thick silica brick. Each furnace was electrically heated with Kanthal wire and equipped with a chromel-alumel thermocouple for monitoring of temperature(Figure 6). All measured temperatures deviated only $\pm$ 5°C from the nominal value. Six graphite molds as shown in Figure 7 were placed within each furnace. The graphite molds were provided with an overflow hold to drain the excess metal out of the mold. Thus all the specimens become equal size of 1/4 inch diameter and 3/4 inch long.

During pouring, the metal stream was divided into the six graphite molds by a pouring basin (Figure 7). Total time of pouring was approximately 46 seconds.

Isothermal Holding of Ductile Iron

Graphite molds with the samples were removed from the holding furnaces at the desired time intervals and quenched in water to arrest the transformation. The isothermal holding time was varied from 10 seconds to 7 hours depending on temperature and composition. The temperatures of the seven holding furnaces were maintained approxiately at 1130, 1050, 1020, 980, 950, 920 and 840°C.

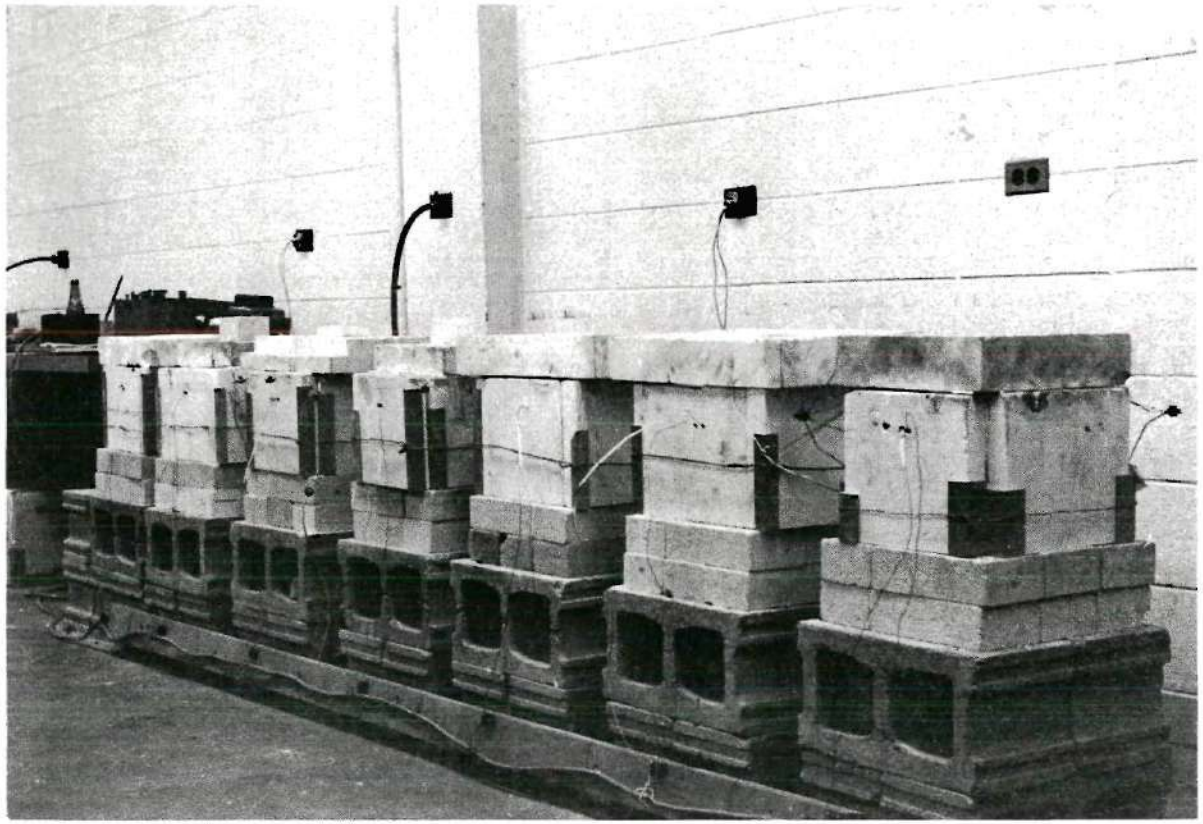

Figure 6. Furnaces for Isothermal Heat Treatment.

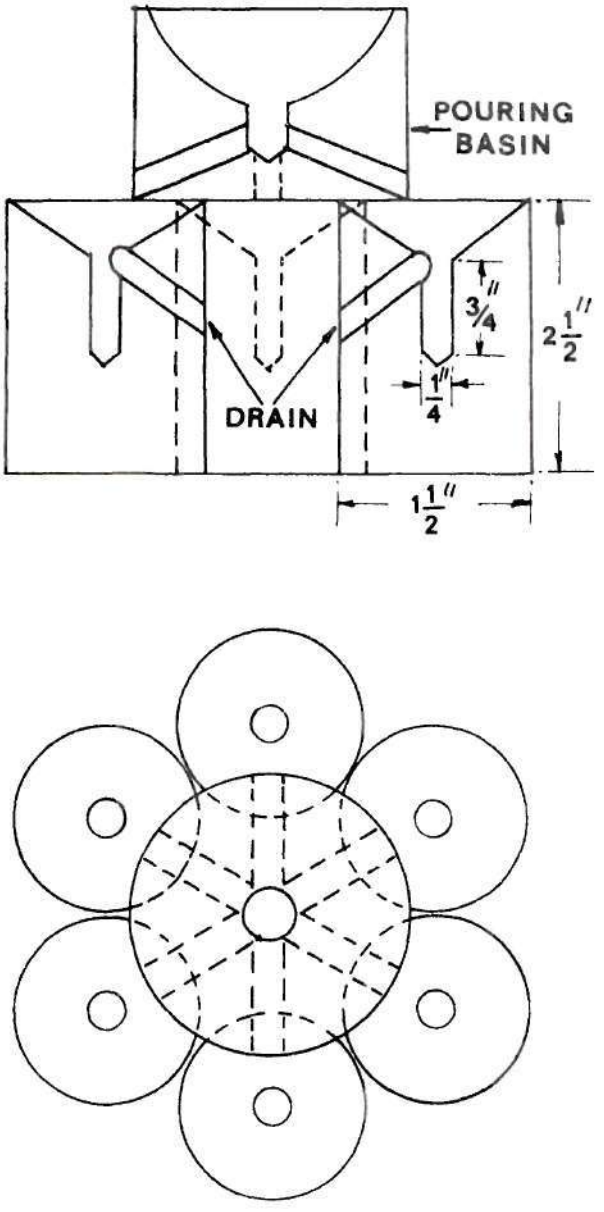

Figure 7. Assembly of Graphite Molds with Pouring Basin.

Casting of Step Bar

In order to study the influence of cooling velocity on the structure of ductile iron, a step bar (Figure 8) was cast in a sand mold. The cooling curve of each section of the step bar was recorded on a Honeywell Multichannel Visicorder using chromel-alumel thermocouples.

Metallographic Investigation

Cylindrical isothermally treated ductile iron samples of 3/4 x 1/4 inch size were ground and polished in several transverse sections as well as in longitudinal section. These specimens were etched in 2 per cent nital and examined under optical microscope.

Different sections of the sand cast step bar were also ground, polished and etched in 2 per cent nital for measurement of the fraction of microconstituents by the point counting method (75,76). The detail procedure of the point counting method is described in Appendix 1.

Measurement of Nucleation and Growth of Graphite Spheroids

In order to study the growth of graphite spheroids under isothermal conditions, the molten iron was poured into a series of graphite molds maintained at 1128 and 950° C in two constant temperature holding furnaces.

In an effort to increase the accuracy of the measurement of nodule diameter, the grinding and polishing were carefully done so that the spherical shape of the graphite particles was essentially

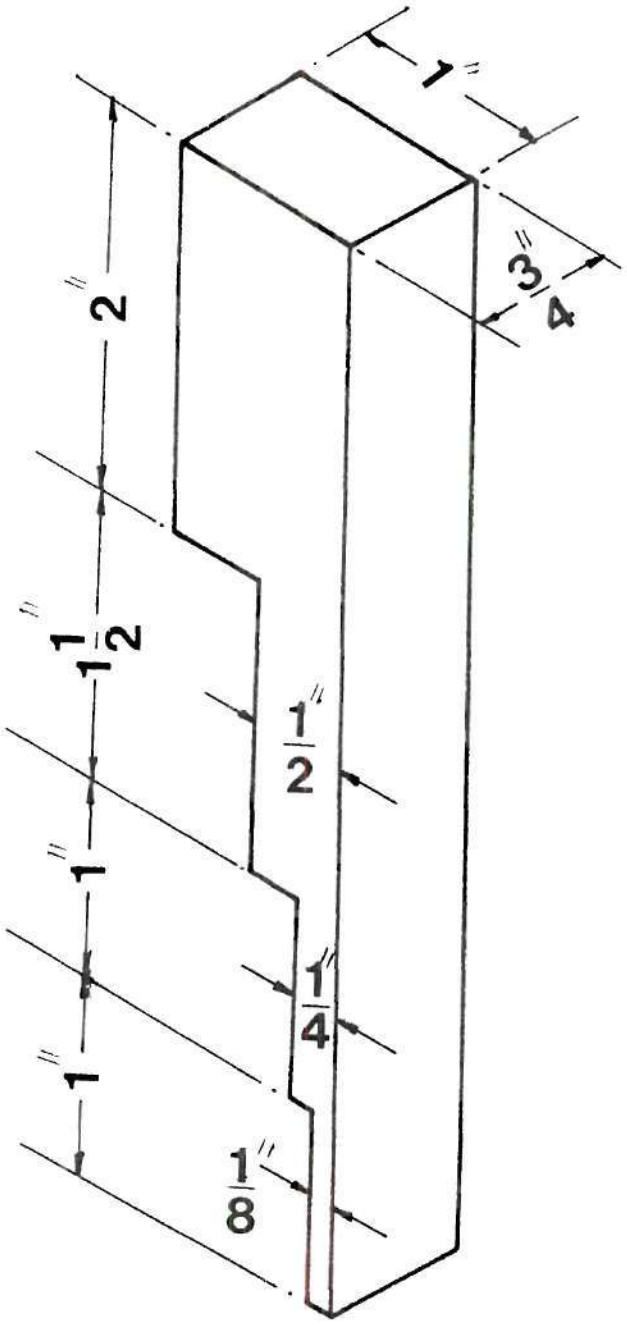

Figure 8. Design of Sand Cast Step Bar.

undisturbed. The number of spheroids were counted from the photomicrographs of five random areas of the unetched sample at X 200.

The average diameter of the graphite particles was calculated by using Schwartz-Saltykov method (75,76). According to this analysis, the particle sizes were first sorted into several groups. If the diameter of the particles in the first size group is Δ, and that of the second group is 2Δ, etc., then the diameter of the maximum sized particle is given by $D_{max} = K\Delta$ where K is the number of groups.

Thus the total number of particle in the first size group can be written as

$$N_A(1) = \sum_{j=1}^{K} N_A(1,j)$$

where the index j designates the group of particles which form the given sections on the plane of polish.

Similarly, the total number of sections of the second size group is:

$$N_A(2) = \sum_{j=2}^{K} N_A(2,j)$$

and so on.

Next, the total number of particles per unit area of the test plane (N_A) is

$$N_A = N_A(1) + N_A(2) + - - - - + N_A(K)$$

The number of spheroids per unit volume was then calculated from the expression

$$N_v = \frac{1}{\Delta} \sum_{i=1}^{K} \alpha_i \, (N_A)_i$$

Where the coefficients α_i are obtained from the table 4 given in Appendix 1.

Finally, the mean diameter of the graphite spheroid is obtained from the expression

$$\bar{D} = \frac{N_A}{N_V} .$$

where N_A = Number of particles per unit area

N_V = Number of particles per unit volume.

Electron Microprobe Analyses

The distributions of C, Si, Mn and Cu in isothermally treated ductile iron specimens were determined by scanning several nodules and the adjacent matrix with the electron beam. The speed of scanning was 12 microns per minute and the beam size in all cases was one micron. Microprobe analyses were done at different times and consequently the concentration profiles of the alloying elements were from different nodules.

CHAPTER IV

RESULTS

Growth of Graphite Spheroids During Process of Solidification

In the present study the number of nodules per unit volume and their average diameter were measured for two different ductile iron heats. One of the ductile iron heats was prepared with normal procedure and the other heat was inoculated with 0.5 per cent FeSi (85% Si) after Mg treatment. This difference in processing cycle causes significant change in the structure and properties of ductile iron. Therefore an attempt has been made to determine quantitatively the variation of some of the structural parameters like nodule count and nodule size with isothermal annealing time.

It can be seen from Figure 9 which illustrates the variation of nodule count and nodule diameter that at temperatures near 1128°C there is a sharp increase in the diameter of the spheroids within the first 360 seconds and thereafter the growth occurs at a slower rate. Simultaneously the number of nodules decreases very rapidly at the beginning and then the decrease takes place at a slower rate.

The microstructures occuring at successive stages of isothermal transformation at 1128°C are shown in Figures 10(a), 10(b), and 10(c). The photomicrograph in Figure 10(a) shows larger nodules surrounded by austenite envelopes and smaller nodules embedded in a ledeburitic

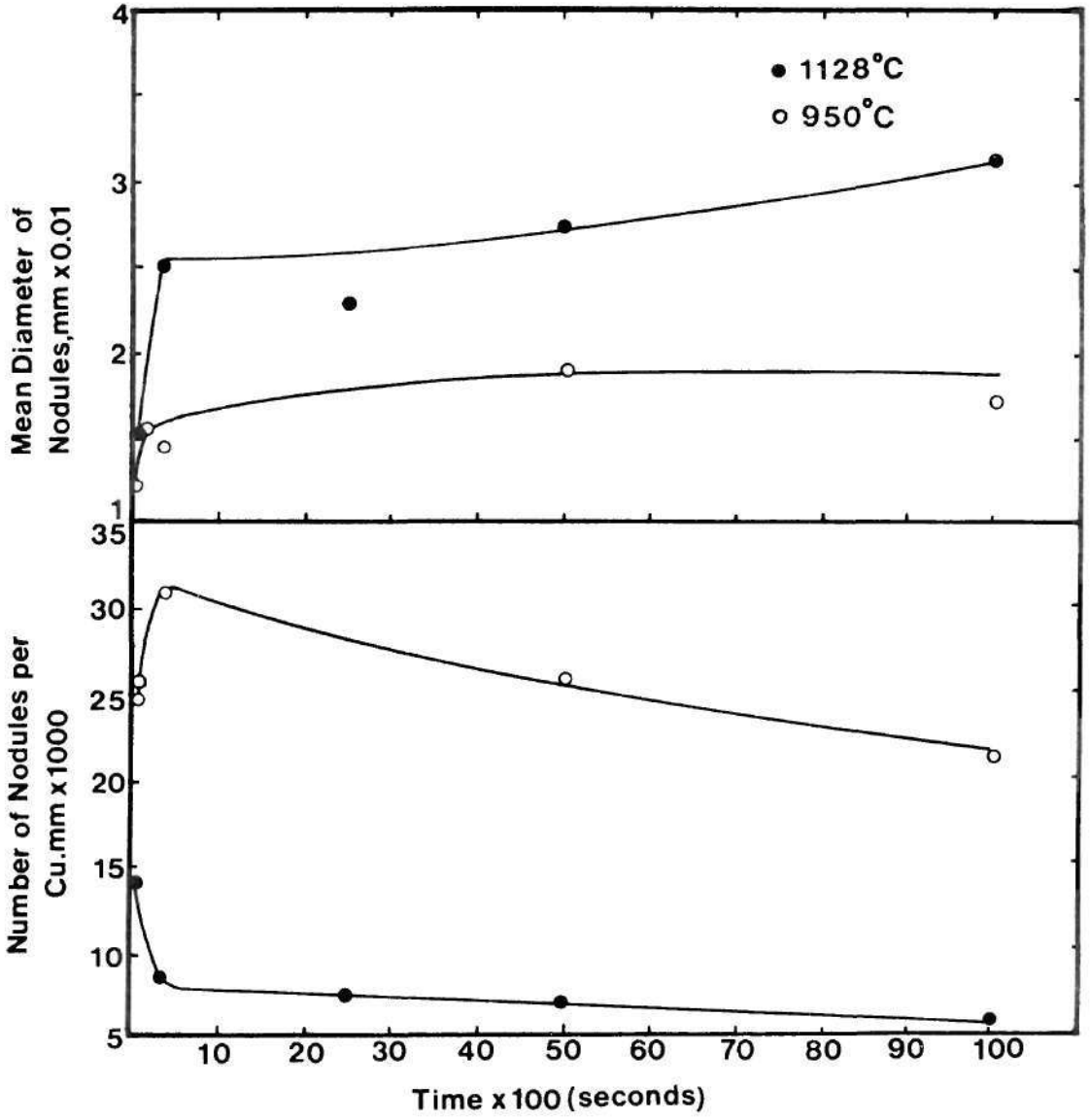

Figure 9. Influence of isothermal holding time on the nucleation and growth of graphite nodules.

(a) 60 Seconds at 1128°C

(b) 2500 Seconds at 1128°C

(c) 10,000 Seconds at 1128°C

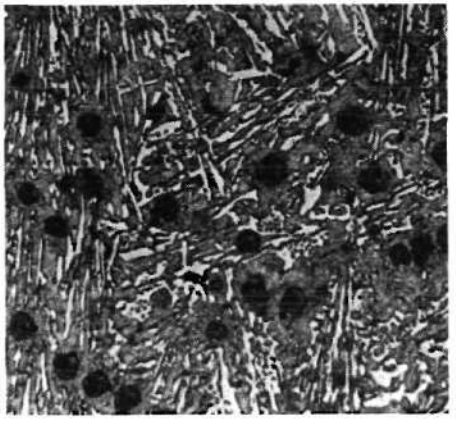

(d) 10 Seconds at 950°C

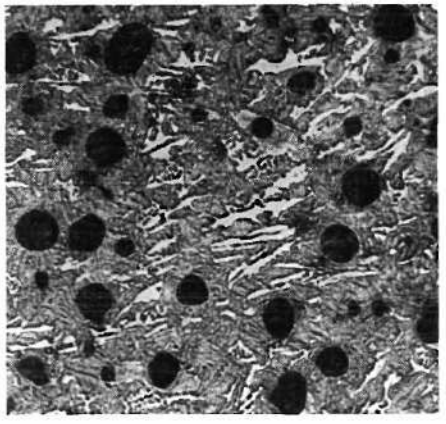

(e) 60 Seconds at 950°C

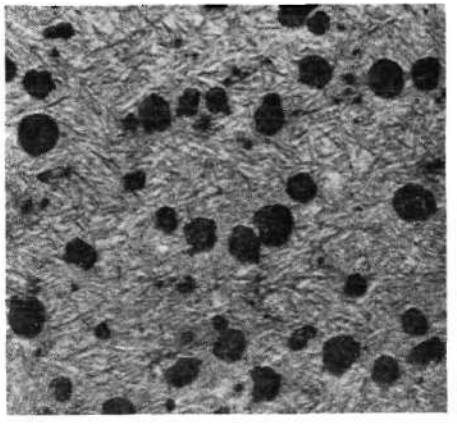

(f) 10,000 Seconds at 950°C

Figure 10. Microstructures of Specimens Isothermally Held at 1128°C and 950°C for Different Time Intervals.

matrix. As the holding time is increased, the ledeburitic cementite dissociates and consequently the amount of ledeburite in the structure decreases as can be seen in Figure 10 (b). Only a few areas of ledeburite are visible at the interstices of graphite-eutectic cell boundaries. In addition, considerable growth of graphite nodules has taken place by the diffusion of carbon from the ledeburitic cementite.

After longer time of holding, the last traces of ledeburitic cementite completely decompose and thereby the graphite spheroids grow slightly as can be seen in Figure 10(c). Due to the quenching of the specimen in water, the austenite surrounding the nodules partially transformed to martensite.

It can be noted from Figures 10(a) and 10(b) that the amount of martensite increases with increasing holding time but the distribution of martensite is not uniform throughout the structure. A close examination of the structure in Figure 10(b) shows the density of martensite needles is much higher near the graphite nodules than the area close to the ledeburite where the carbon content is relatively high. With prolonged annealing at 1128°C, the last trace of the ledeburite is dissolved in the austenite matrix and the austenite becomes homogeneous with respect to carbon content. As a result uniformly distributed martensite needles are observed in the structure illustrated in Figure 10(c).

Isothermal growth of graphite at lower temperature around 950°C occurs at a very fast rate at an earlier stage and then the growth rate diminishes and eventually approaches zero with longer holding time.

The nodule count, however, goes up in the first 60 seconds and then tends to decrease with longer holding time.

The phase transformations at 950°C are illustrated in Figures 10(d), 10(e) and 10(f). The structure of the specimen isothermally treated at 950°C for 10 seconds is shown in Figure 10(d). Only smaller graphite spheroids in a matrix of cementite and martensite (partly decomposed ledeburite) are visible. After 60 seconds the cementite decomposes further resulting in an increase in the size of the spheroids which can be seen from Figure 10(e). The cementite is completely decomposed after 10,000 seconds but the graphite spheroids remain essentially unchanged (Figure 10(f)).

The equilibrium carbon content of the austenite at 950°C is close to the eutectoid composition and is much lower than that at 1128°C. Consequently the austenite transforms to fine martensite on quenching in water and the structure is practically free from retained austenite.

Influence of Post-Inoculation on the Nucleation and Growth of Graphite

Figure 11 illustrates the influence of post-inoculation on the nodule number and nodule size of ductile iron isothermally held at 1135°C for different time intervals. It can be seen from this graph that the diameter of the nodule grows within the first 45 seconds and thereafter the size of the nodule does not change significantly.

On the otherhand the number of nodules decreases abruptly at the beginning and then it remains essentially constant.

A comparison of the nodule size and the nodule number curves for normal and post-inoculated iron shows that the nodule count is much

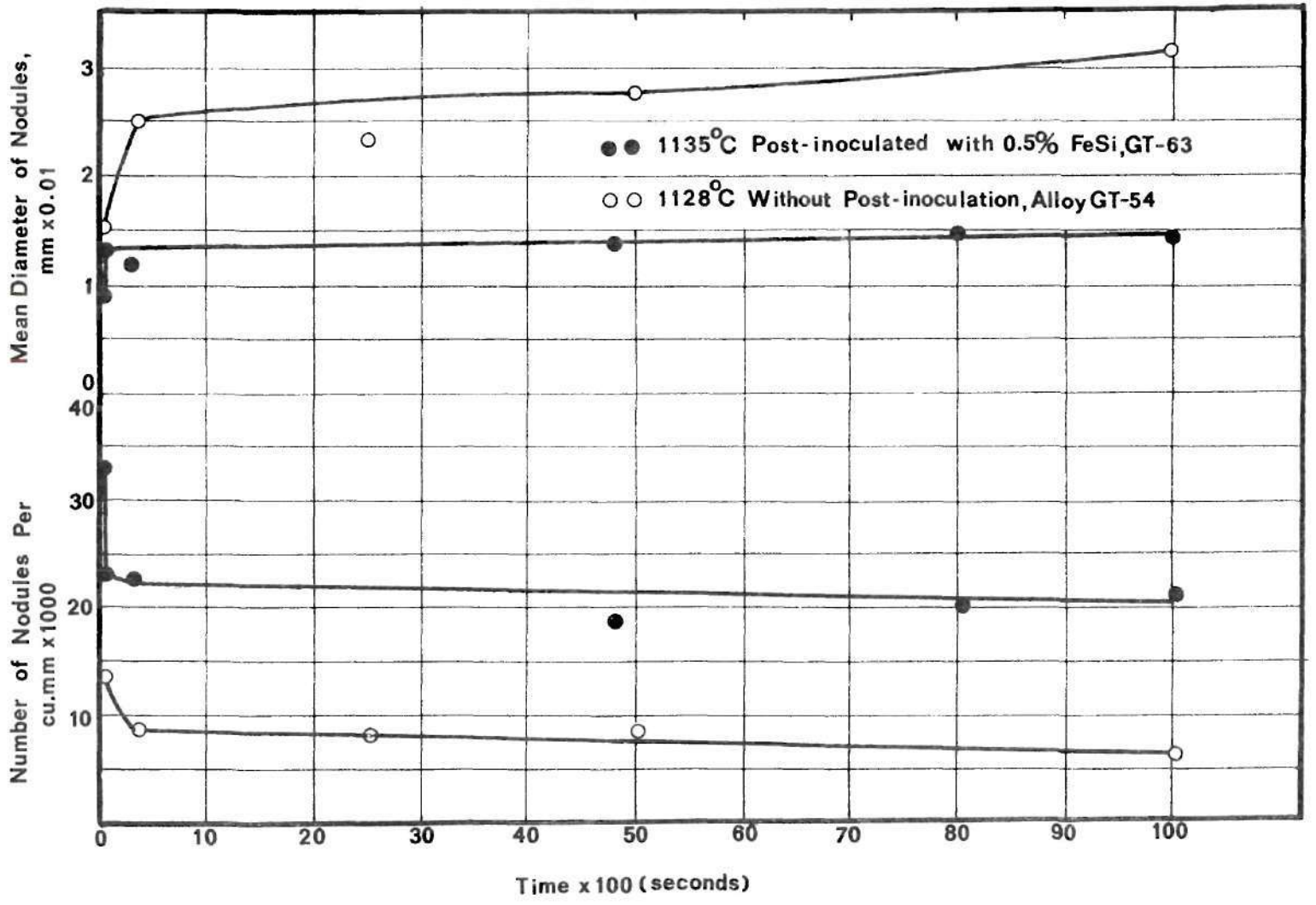

Figure 11. Influence of Post-Inoculation on the Nucleation and Growth of Graphite Nodules.

higher in the post-inoculated iron and consequently the average diameter of the nodules in post-inoculated iron is smaller than the iron having no post-inoculation treatment. This can also be noted from the microstructures in Figures 10 and 12.

Structural Changes at Different Isothermal Temperatures

Results of the isothermal transformations are summarized in the T-T-T curves which are determined by observing a large number of specimens at a series of temperatures.

The time for completion of cementite dissociation reaction is based upon the structure in which the amount of cementite is less than 1.0 per cent. Influence of alloying elements is illustrated by plotting T-T-T curves of alloys with increasing alloy content on the same graph.

Figure 13 represents the T-T-T curve of the melt GT-51 containing 3.70 per cent C, 1.95 per cent Si and 0.84 per cent Mn. It can be seen from this figure that the dissociation of cementite takes place in the shortest time at temperatures around 980°C. The time for completion of the reaction, however, increases as the isothermal reaction temperature is raised above or lowered below 980°C.

When the melt is quenched down to the temperature 1128°C, just below the eutectic, graphite nodules have probably precipitated in the liquid state depleting the surroundings of carbon which initiates precipitation of austenite around the graphite. The remaining liquid transforms to ledeburite which can be seen from Figure 14(a).

Transformation at longer periods is accompanied by dissociation of cementite and precipitation of carbon on the existing graphite

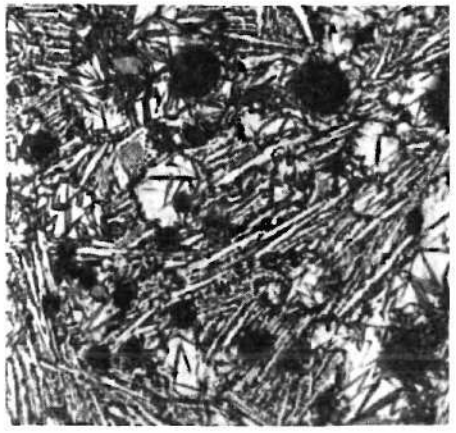

(a) 60 Seconds at 1128°C

(b) 2500 Seconds at 1128°C

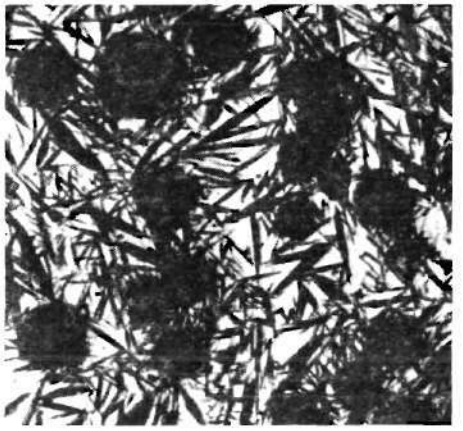

(c) 10,000 Seconds at 1128°C

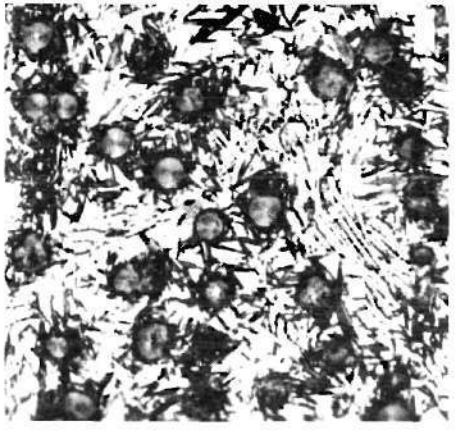

(d) 13 Seconds at 1135°C

(e) 45 Seconds at 1135°C

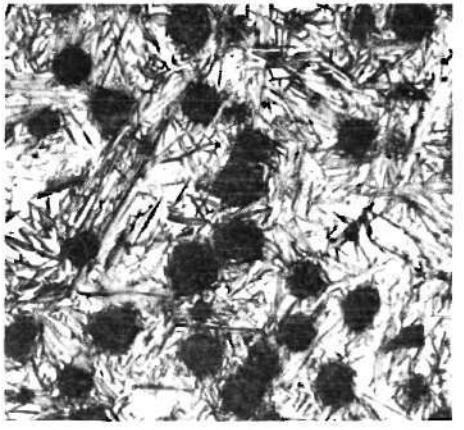

(f) 10,000 Seconds at 1135°C

Figure 12. Microstructures of the Specimens Isothermally Held at 1135°C and 1128°C for Different Time Intervals.

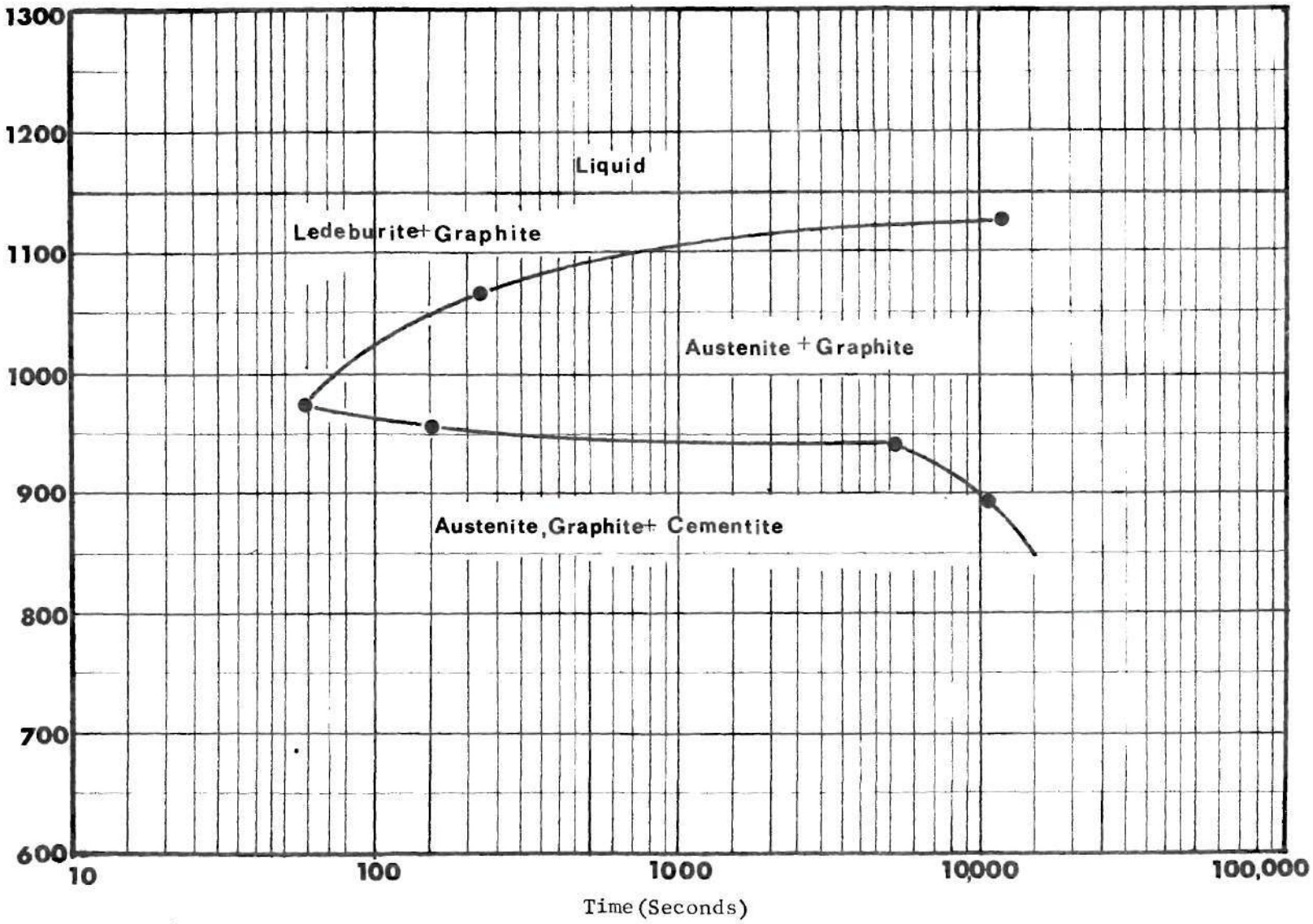

Figure 13. Time-Temperature-Transformation Curve for Decomposition of Cementite in Ductile Iron. (C-3.70, Si-1.95, Mn-0.84, Mg-0.03, S-0.03).

Figure 14(a) Alloy GT-51, 2 minutes at 1128°C, 2% Nital, x200.

14(b) Alloy GT-51, 81 Minutes at 1128°C, 2% Nital, x200.

14(c) Alloy GT-51, 180 Minutes at 1128°C, 2% Nital, x 200.

spheroids. Thus the amount of ledeburite in the structure decreases with increasing holding time (Figure 14(b)). Owing to the decomposition of cementite, a carbon concentration gradient is set up within the austenite with the concentration of carbon being higher close to the cementite and lower adjacent to the graphite spheroid. This results in a non-uniform distribution of martensite needles in the structure (Figure 14(b). Fine martensite needles are formed at the carbon depleted austenite/graphite interface and coarse martensite plates are formed in the relatively high carbon content matrix away from the graphite nodules. Martensite needles formed at the austenite/graphite interface are not so sharply defined; instead they have an angular appearance (77,78). It can also be noted in the Figure 14(b) that at the interface of the ledeburite and the austenite, a thin layer of fine martensite has formed. This is due to the stress developed in austenite during quenching of the specimen in water. At 1128°C the dissociation of cementite is completed after 180 minutes (Figure 14(c)). After this prolonged isothermal holding, the structure consists of graphite, austenite and uniformly distributed martensite.

Figures 15(a) and 15(b) represent the structure of the specimens which were held at 980°C for 15 and 60 seconds respectively and then quenched in water. The specimen which was held for only 15 seconds consists of a few graphite nodules in a ledeburitic matrix whereas the specimen held for 60 seconds consists of large number of graphite nodules in a matrix of fine martensite and austenite. Since the M_s and M_f temperatures are raised due to the lowering of carbon content

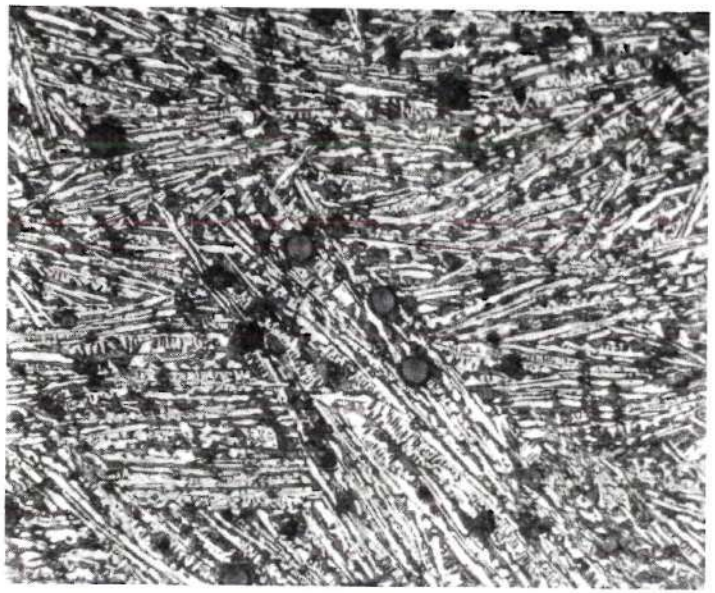

Figure 15(a). Alloy GT-51, 15 Seconds at 980°C, 2% Nital, x200.

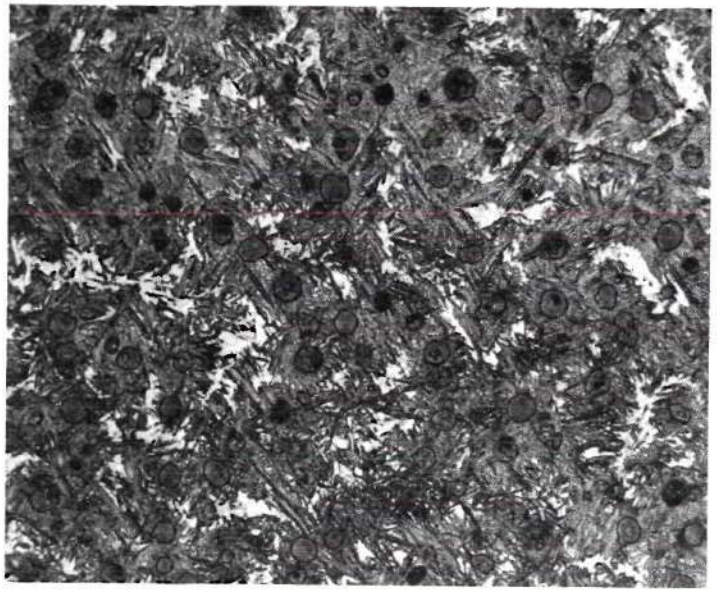

Figure 15(b). Alloy GT-51, 60 Seconds at 980°C, 2% Nital, x 200.

with decreasing temperature, the microstructure of the specimen quenched from 980°C after 60 seconds shows only small areas of retained austenite (Figure 15(b)) as compared to the specimen quenched from 1128°C after 2 minutes (Figure 14(a)).

Lowering of isothermal temperature below 980°C, the time required for the cementite breakdown is considerably increased. Figures 16(a), 16(b) and 16(c) show the structures of the specimens held for 2, 124 and 230 minutes at 845°C. It is clear from this structure that the rate of decomposition of cementite is very slow at this lower temperature. The cementite breakdown times at 1128°C, 980°C, 845°C are 180, 1, and 230 minutes respectively.

A comparison of Figures 14, 15 and 16 indicates that the size of the graphite spheroid is maximum at 1128°C. At this temperature, the structure contains fewer but larger graphite spheroids. When the specimens are isothermally treated at the lower temperature range (980°C to 845°C), the nodules become smaller in size and larger in number.

Apart from number and size of the graphite, the shape of the graphite also changes with the lowering of temperature. In the temperature range 1128°C to 980°C the spherical shape is well maintained but at lower temperatures around 845°C the shape of the graphite is not exactly spherical as can be seen from Figures 16(b) and 16(c).

Influence of Alloying Elements on the T-T-T Curve

Effect of Si, Mn, Cr and Cu has been investigated in this work. Si is a strong graphitizer and is expected to accelerate the speed of cementite breakdown. On the otherhand, Mn and Cr stabilize carbide,

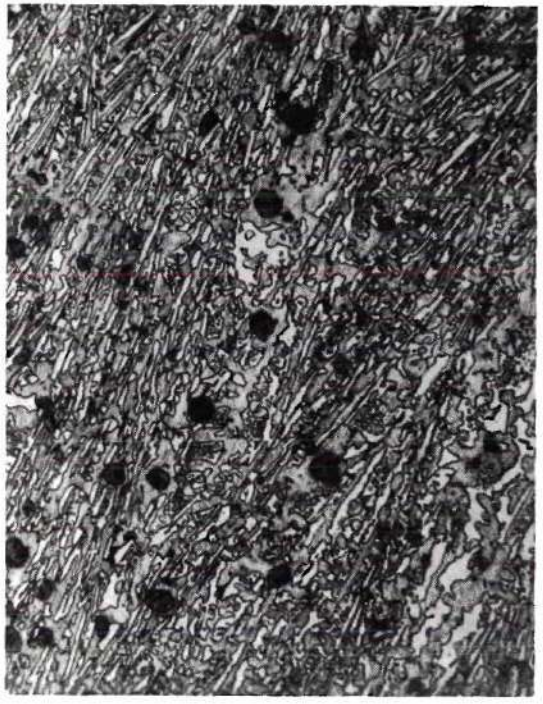

Figure 16(a) Alloy GT-51, 2 Minutes at 845°C, 2% Nital x 200.

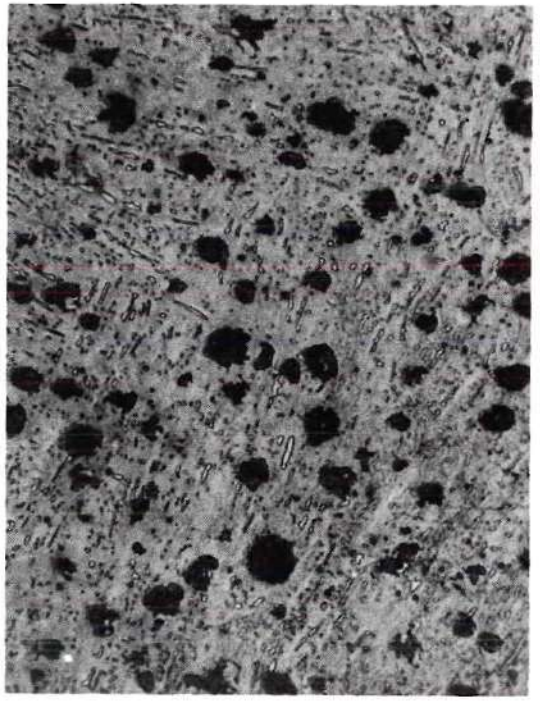

16(b) Alloy GT-51, 124 Minutes at 845°C, 2% Nital, x 200.

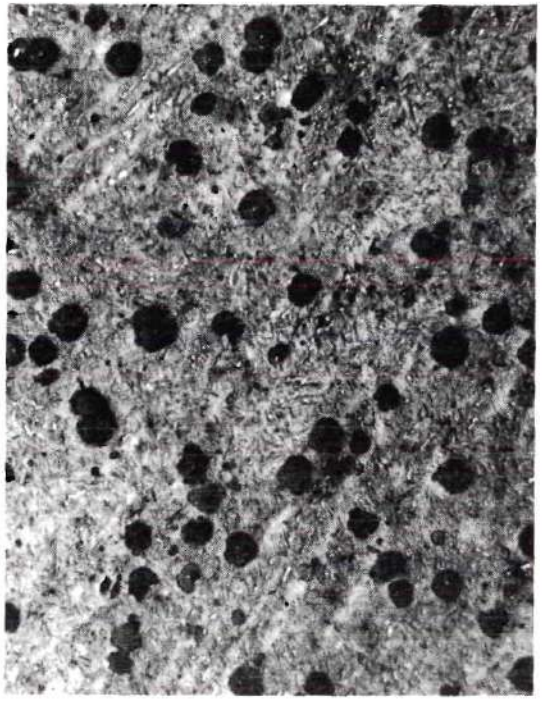

16(c) Alloy GT-51, 230 Minutes at 845°C, 2% Nital, x 200.

therefore, they will retard the dissociation of cementite. Cu is added as a pearlite promoting agent in ductile iron. If the relative graphitizing power of Si is taken as 1.0, the corresponding graphitizing power of Cu would be approximately 0.25 (68,69). Here the term "graphitizing power" implies the ability of the alloy element to enhance the rate of decomposition of carbide. Thus Cu does not have any significant influence on the dissociation of carbide. The effect of each alloying element is presented by a series of T-T-T curves in the following:

Effect of Si

Addition of Si enhances the speed of cementite decomposition and thereby shifts the T-T-T curve to the left side (Figure 17). At temperatures around 980°C, the cementite is completely decomposed within 38 seconds when the Si content is 4.10 per cent. The decomposition of cementite in alloy GT-52 is accelerated relatively more at temperatures above and below 980°C.

Effect of Mn

The cementite decomposition reaction is considerably retarded with increased Mn content in the alloy as can be seen from Figure 18. Increasing the Mn content from 0.84 to 1.62 per cent, the T-T-T curve is shifted to the right and the curve moves further to the right as the Mn content is increased to 2.05 per cent.

In addition to stabilizing cementite, Mn also stabilizes austenite. Figures 19 and 14(b) show the microstructures of the specimens held at temperatures around 1128°C for 71 to 81 minutes. It is clear from these structures that the amount of retained austenite in the speci-

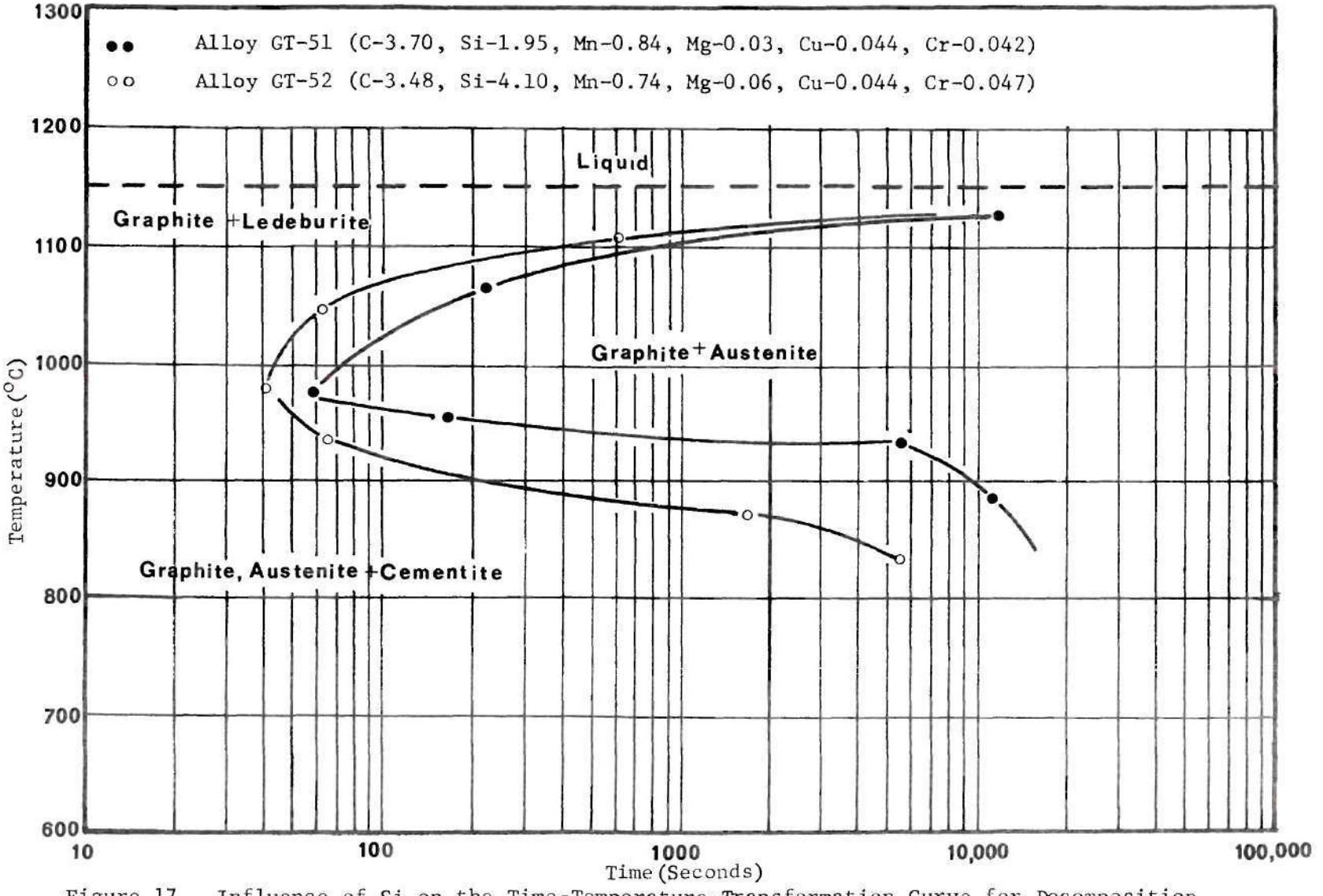

Figure 17. Influence of Si on the Time-Temperature-Transformation Curve for Decomposition of Cementite in Ductile Iron.

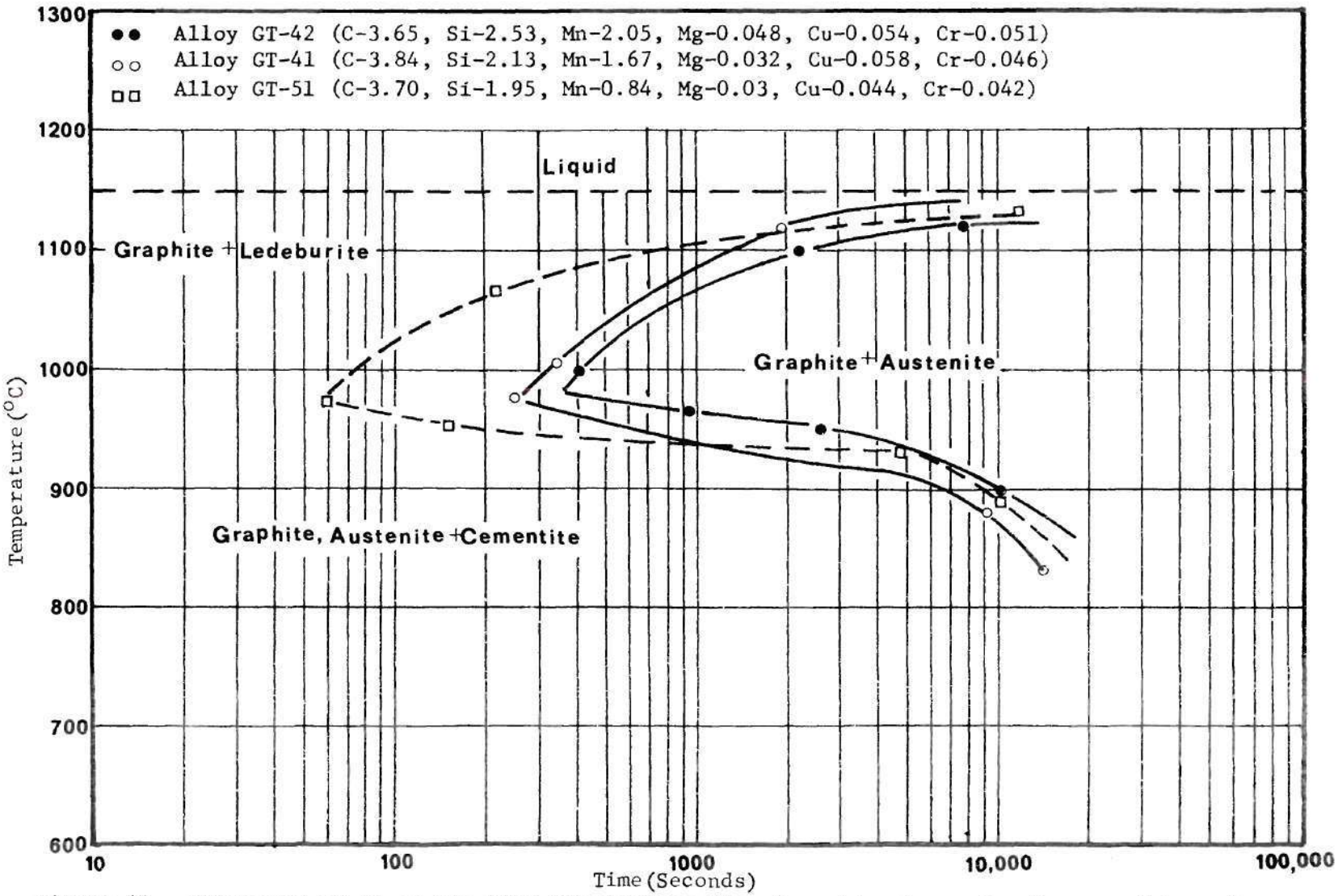

Figure 18. Influence of Mn on the Time-Temperature-Transformation Curve for Decomposition of Cementite in Ductile Iron.

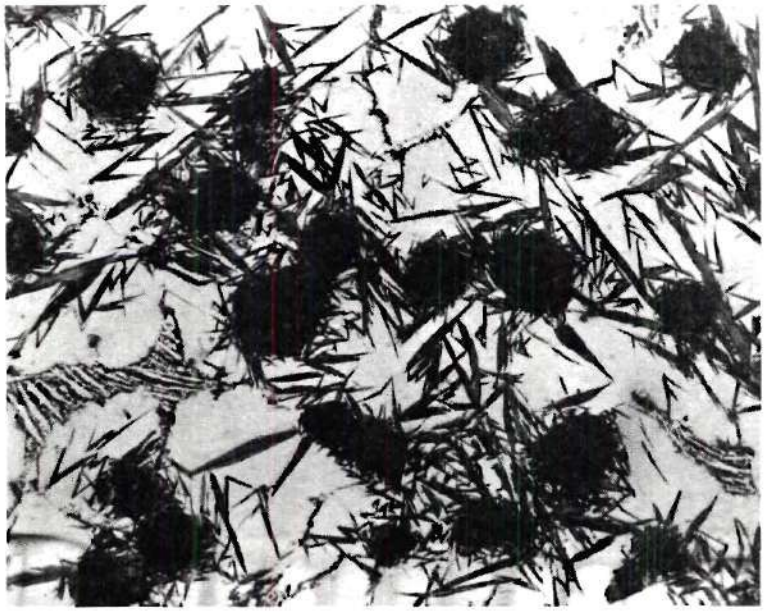

Figure 19. Alloy GT-41, 71 minutes at 1128°C, 2% Nital, x200.

men with 0.84 per cent Mn is less than that of the specimen with 1.67 per cent Mn.

Effect of Cr

Presence of small amounts of Cr severely retard the decomposition of cementite as evident from Figure 20. The T-T-T curve is shifted to the right and the nose of the curve is also raised to around 1045°C. At this temperature, the carbide decomposes within 6.5 minutes compared to 1.0 minute in alloy (GT-64) containing negligible amount of Cr. As expected, the speed of cementite decomposition is also retarded at higher and lower temperatures.

Effect of Cu

The influence of Cu on the T-T-T curves for the alloys containing 1.07 and 2.13 per cent respectively is shown in Figure 21. Since Cu is a mild graphitizer (68,69) at the solidification stage, the T-T-T curve for decomposition of cementite is not shifted by higher addition of Cu. Unlike Si and Mn, Cu raises the nose of the T-T-T curve to about 1080°C at which temperature the structure becomes free from cementite within 70 to 80 seconds depending on Cu content.

Cu also exerts a refining effect on the ledeburite as well as on the graphite. The ledeburite in the microstructure of the specimen containing 1.07 per cent Cu is relatively finer than that of specimen containing negligible amounts of Cu (Figures 14(a) and 22). Apart from refining the ledeburite eutectic, Cu reduces the growth rate of graphite spheroid as can be seen from Figure 22.

men with 0.84 per cent Mn is less than that of the specimen with 1.67 per cent Mn.

Effect of Cr

Presence of small amounts of Cr severely retard the decomposition of cementite as evident from Figure 20. The T-T-T curve is shifted to the right and the nose of the curve is also raised to around 1045°C. At this temperature, the carbide decomposes within 6.5 minutes compared to 1.0 minute in alloy (GT-64) containing negligible amount of Cr. As expected, the speed of cementite decomposition is also retarded at higher and lower temperatures.

Effect of Cu

The influence of Cu on the T-T-T curves for the alloys containing 1.07 and 2.13 per cent respectively is shown in Figure 21. Since Cu is a mild graphitizer (68,69) at the solidification stage, the T-T-T curve for decomposition of cementite is not shifted by higher addition of Cu. Unlike Si and Mn, Cu raises the nose of the T-T-T curve to about 1080°C at which temperature the structure becomes free from cementite within 70 to 80 seconds depending on Cu content.

Cu also exerts a refining effect on the ledeburite as well as on the graphite. The ledeburite in the microstructure of the specimen containing 1.07 per cent Cu is relatively finer than that of specimen containing negligible amounts of Cu (Figures 14(a) and 22). Apart from refining the ledeburite eutectic, Cu reduces the growth rate of graphite spheroid as can be seen from Figure 22.

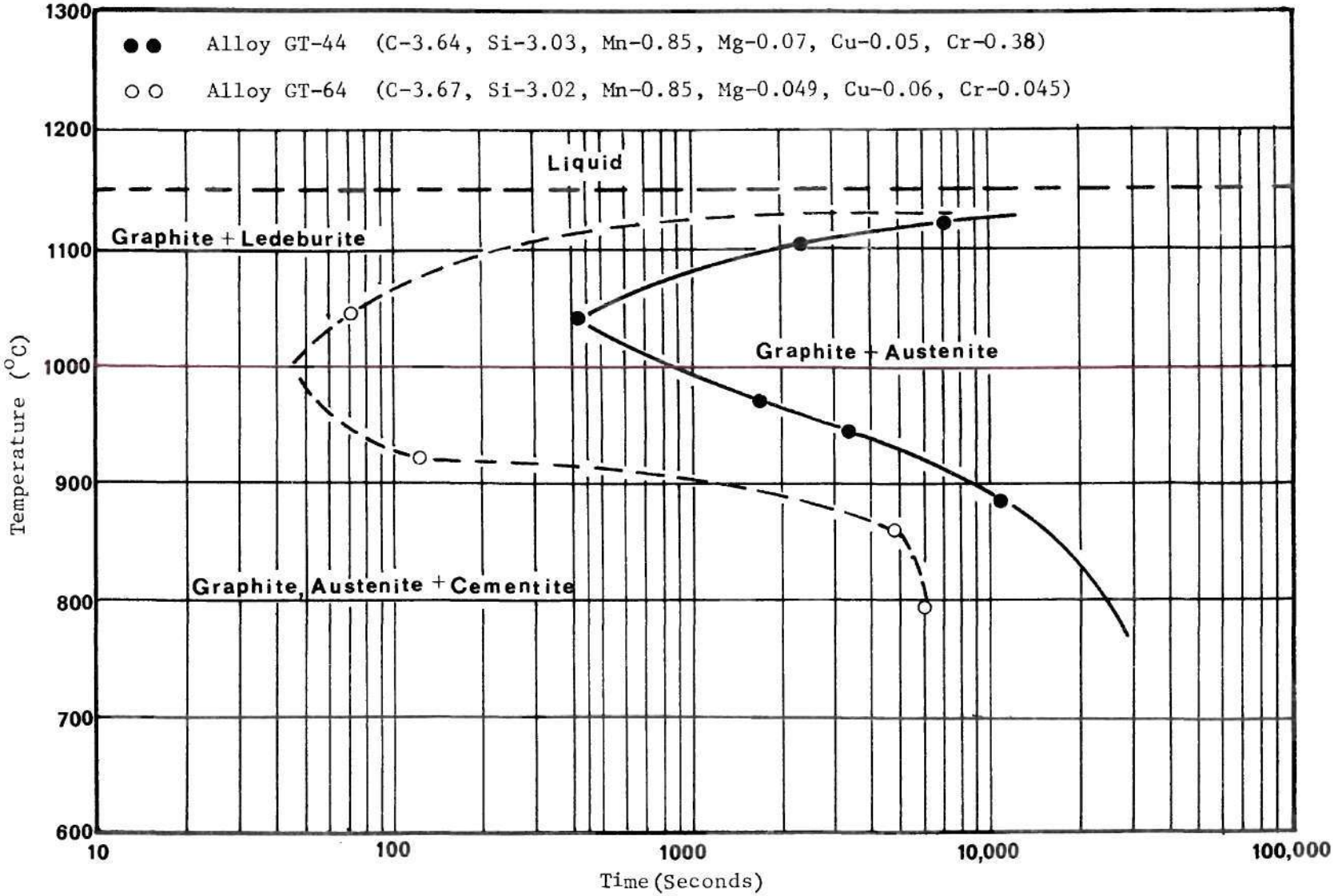

Figure 20. Influence of Cr on the Time-Temperature-Transformation Curve for Decomposition of Cementite in Ductile Iron.

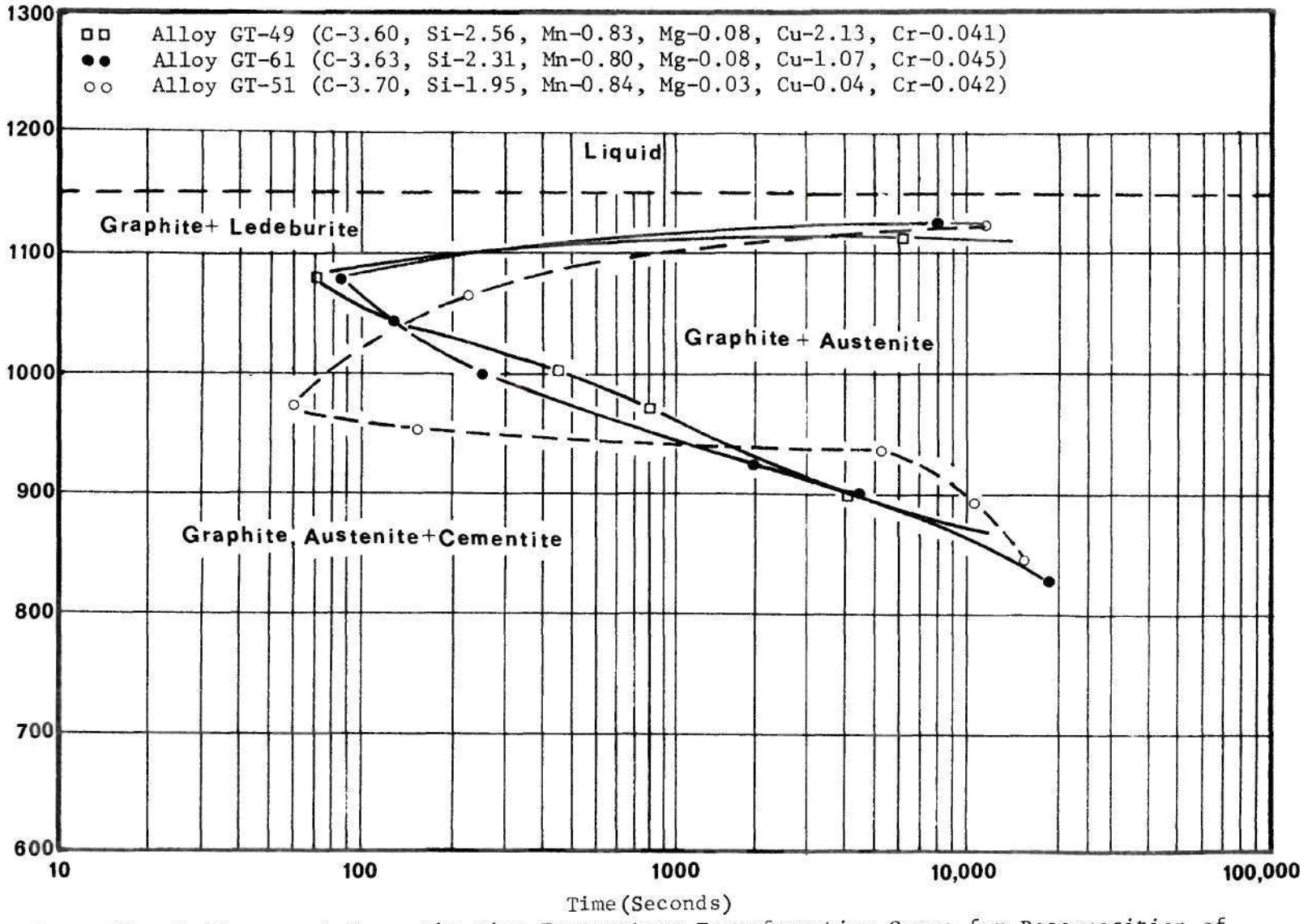

Figure 21. Influence of Cu on the Time-Temperature-Transformation Curve for Decomposition of Cementite in Ductile Iron.

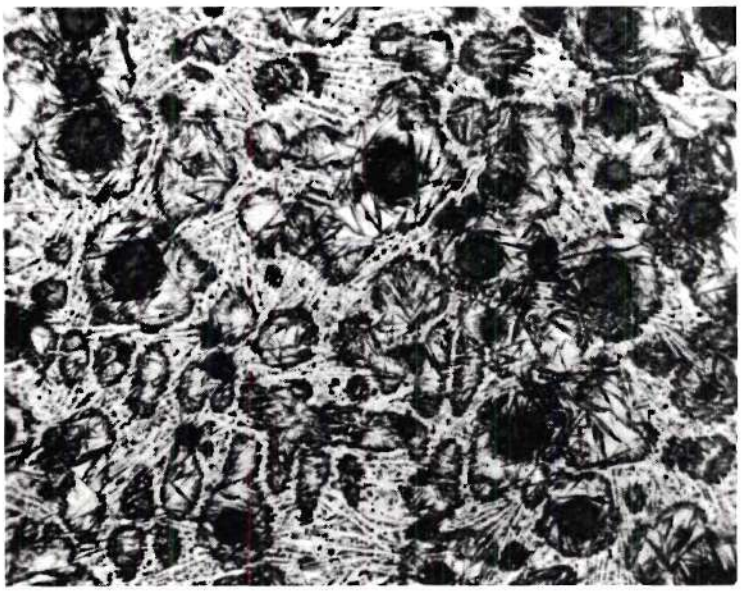

Figure 22. Alloy GT-61, 79 Seconds at 1130°C, 2% Nital, x 200.

Influence of Post-Inoculation on T-T-T Curve

The influence of post-inoculation with FeSi after Mg treatment is two-fold (39). Primarily it enhances the number of effective graphite nuclei and produces more regularly shaped graphite spheroids. Besides there is a substantial reduction of cementite beyond what would have been obtained with equivalent amount of Si addition prior to Mg treatment.

Figure 23 exhibits the influence of post-inoculation on the T-T-T curve for the alloys GT-59, 60 and 62. Si additions to these alloys were made in such a way that the final carbon equivalent of the metals were within 4.35-4.60. Thereby the influence of different amounts of post-inoculant additions has been compared at nearly similar compositions. It is obvious from Figure 23 that the speed of cementite decomposition is much faster in post-inoculated iron than that of the iron in which Si addition was made prior to Mg treatment.

Furthermore, the speed of cementite dissociation increases when the amounts of FeSi addition is increased from 0.3 to 0.5 per cent. However, there is no significant increase on the speed of cementite decomposition when the FeSi addition is further increased to 1.0 per cent.

Another interesting observation in Figures 17 and 23 is the considerable enhancement in the speed of cementite decomposition with lower amounts of Si in post-inoculated iron. If the Si addition is made prior to the Mg treatment, about 1.5 times as much as Si is necessary to obtain the same graphitizing effect. In post-inoculated iron with 2.71 per cent Si, the cementite is completely decomposed

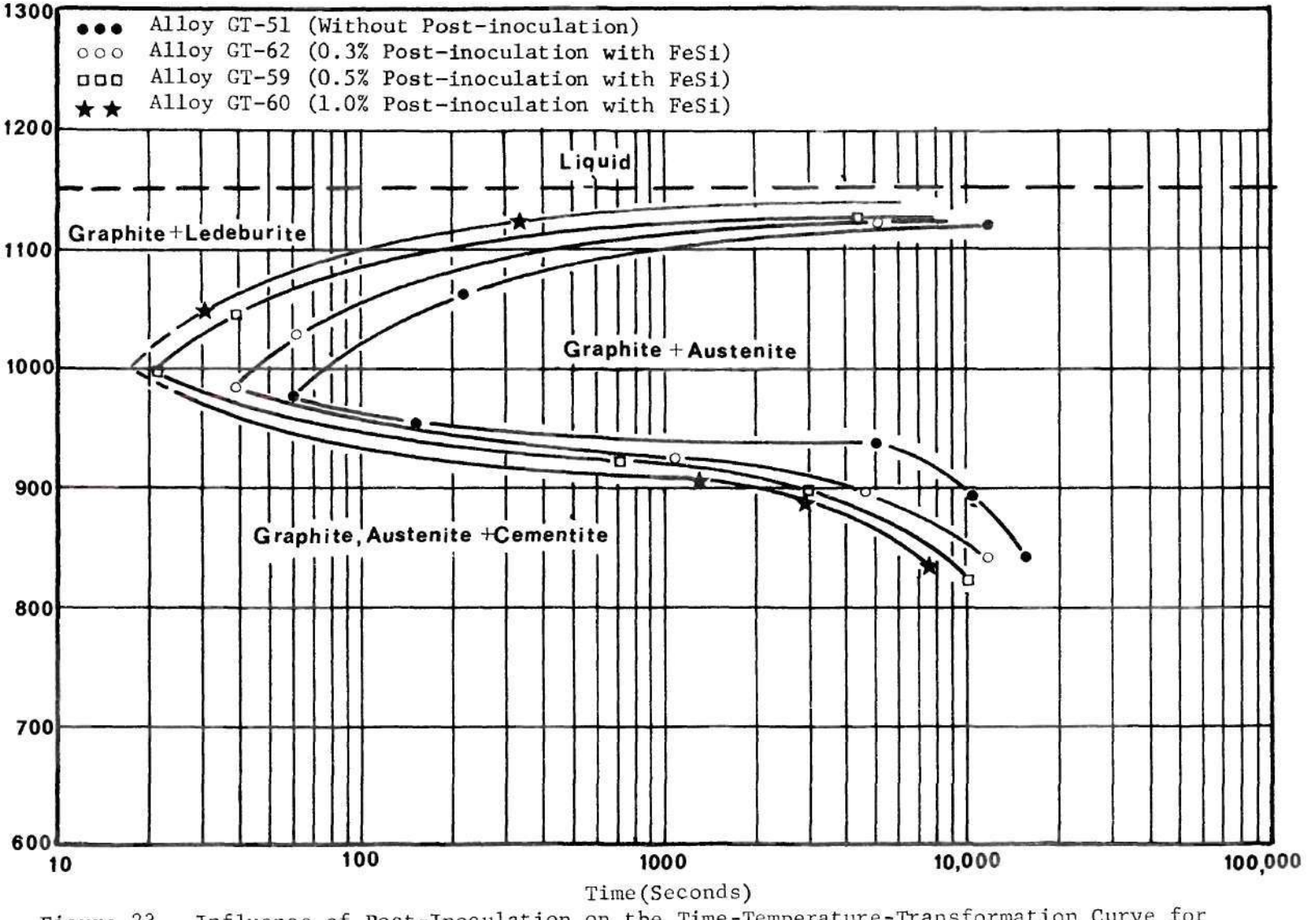

Figure 23. Influence of Post-Inoculation on the Time-Temperature-Transformation Curve for Decomposition of Cementite in Ductile Iron.

within 40 seconds at temperatures near 980°C.

By contrast, the same time is necessary for decomposition of cementite in iron containing 4.10 per cent Si and having no post-inoculation treatment.

Apart from influencing the speed of cementite decomposition, post-inoculation treatment increases the nodule number and reduces the nodule size. This is reflected in Figure 24 which shows that for a particular section thickness the number of nodules/unit volume is higher for post-inoculated iron and that the number of nodules increases with lowering of section thickness. The average diameter of the nodule is smaller in post-inoculated iron and the nodule size increases with increase in section thickness.

Besides influencing the nodule number and nodule size, addition of FeSi after Mg treatment greatly alters the structure of the matrix. Quantitative measurements of ferrite, pearlite and carbide in 1/8 x 3/4, 1/4 x 3/4, 1/2 x 3/4 and 1 x 3/4 inch sections of sand cast step bars have been made and plotted against the corresponding section thickness (Figure 25).

The accelerating influence of post inoculation on the reduction of cementite in the structure can be seen from Figure 25 which shows that in thin section (1/8 x 3/4) the amount of carbide is reduced from 38 to 8 per cent and in higher sections carbide is completely eliminated from the structure.

Furthermore, in post-inoculated iron there is a progressive increase in the amount of ferrite and a decrease in the amount of pearlite with increasing section sizes. Whereas the pearlite content

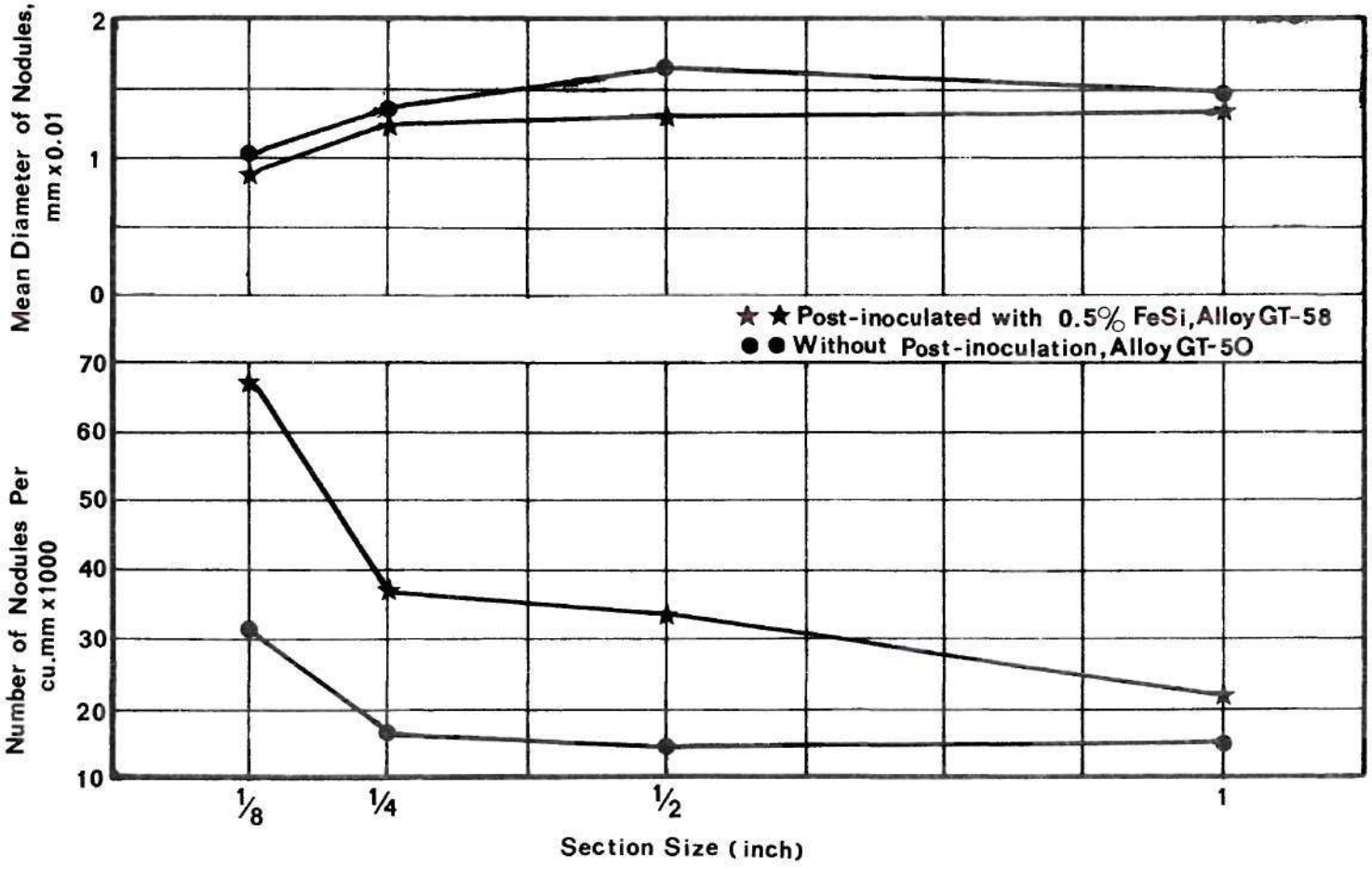

Figure 24. Effect of Post-Inoculation on the Nodule Number and Average Nodule Size at Different Section Sizes.

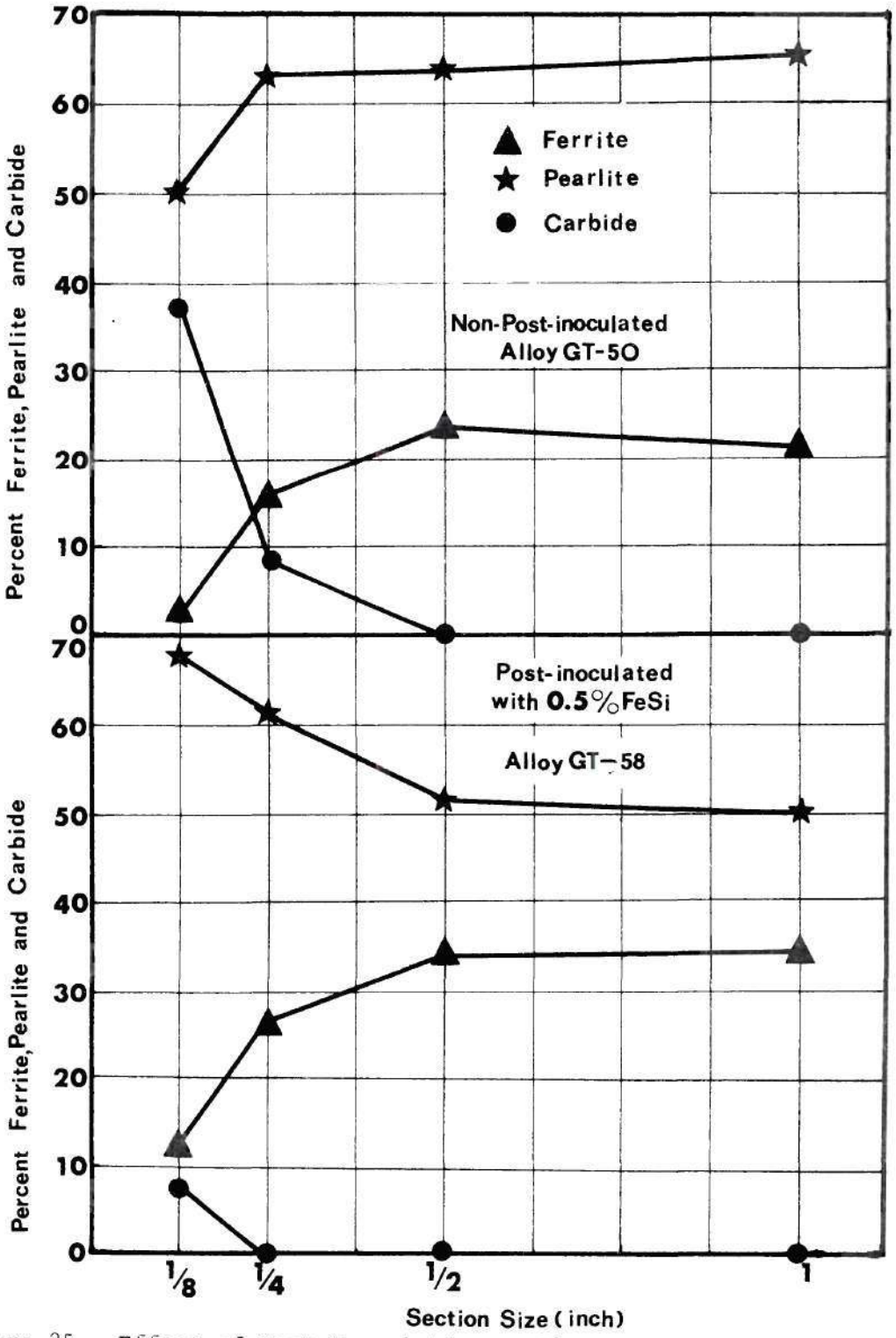

Figure 25. Effect of Post-Inoculation on the Percentage Ferrite, Pearlite and Carbide at Different Section Sizes.

of the iron without post-inoculation, increases with increasing section sizes. By contrast, the amount of ferrite goes up with higher section sizes but it is still lower than that of the post-inoculated iron.

Correlation Between T-T-T Curve and The Cooling Curve

It is possible to predict the structure of ductile iron by superimposing the cooling curves of different section sizes of a sand cast step bar on the T-T-T curve for decomposition of cementite. In Figure 26 the cooling curve of an alloy GT-58 with carbon equivalent of 4.50 is superimposed on the T-T-T curve of alloy GT-59 with almost the same C.E. 4.60. According to the Figure 26 the cooling curve for 1/8 x 3/4 inch section size does not cut the nose of the T-T-T curve for cementite breakdown and therefore some residual carbide should be expected in the structure. Figure 27(a) shows cementite in addition to pearlite, ferrite, and graphite. On the otherhand, the cooling curve for 1/2 x 3/4 inch section cuts the nose of the T-T-T curve and accordingly, the structure is expected to be free from cementite. This result can be seen from Figure 27(b).

Electron Microprobe Studies of the Graphite Nodule and the Matrix Structure

Electron microprobe analyses were performed on the quenched specimens to determine the distribution of C, Si, Mn and Cu in graphite and in the vicinity of the solid/liquid interface. The distributions of C, Si and Mn were determined on specimens (GT-41) held for 30 and 71 minutes at 1128°C. Besides Si and Mn, the distribution of Cu was also determined on iron alloyed with 1.07 per cent Cu (GT-61) and

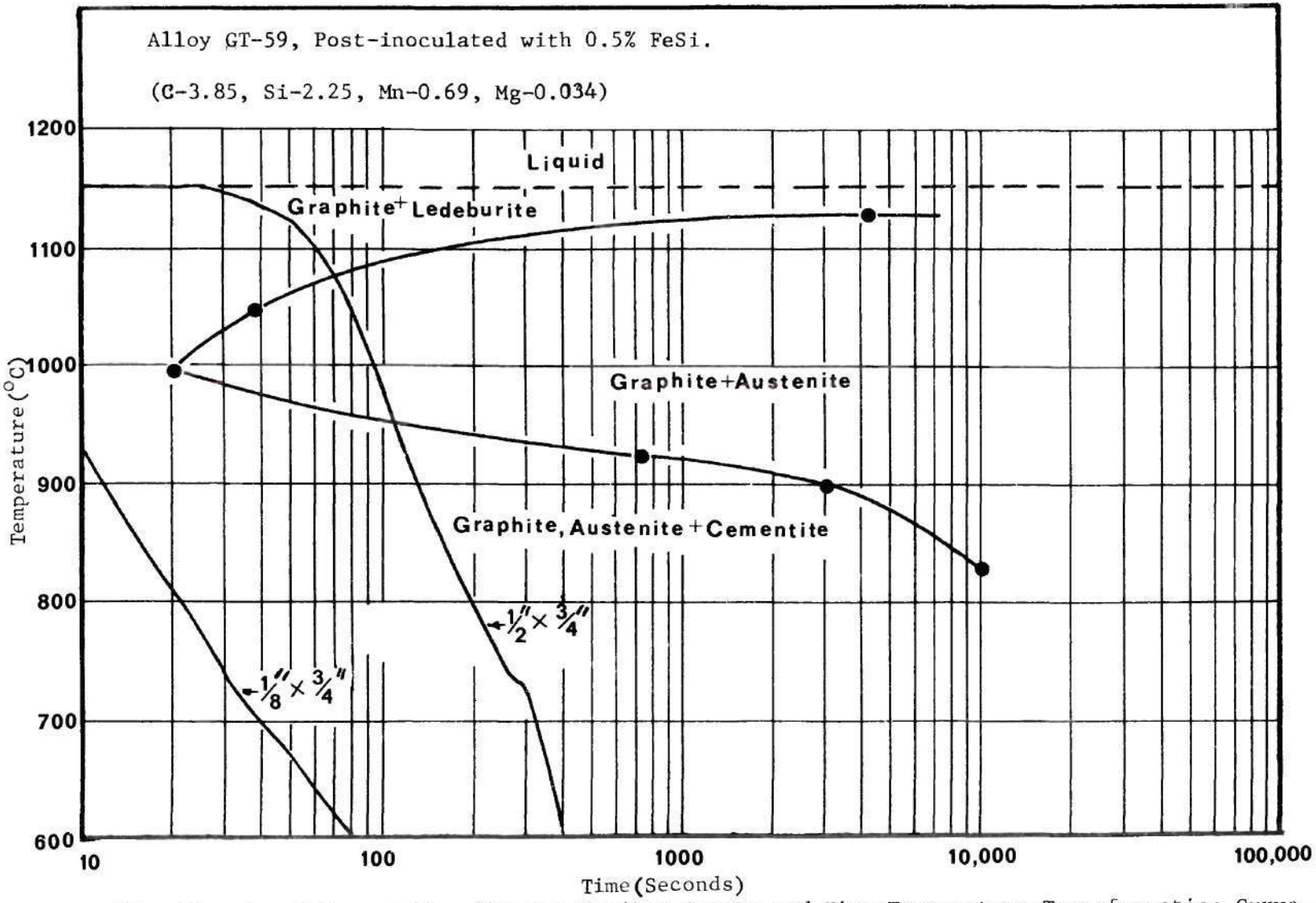

Figure 26. Structural Correlation Between Cooling Curves and Time-Temperature-Transformation Curve.

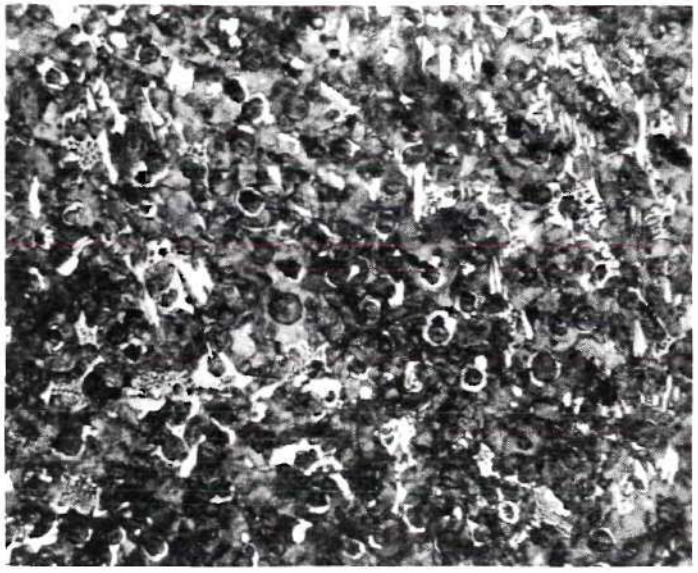

Figure 27(a) Alloy GT-58, 1/8 x 3/4 Inch Section, 2% Nital, x 200. (GT-58, C-3.70, Si-2.37, Mn-0.69, Mg-0.057).

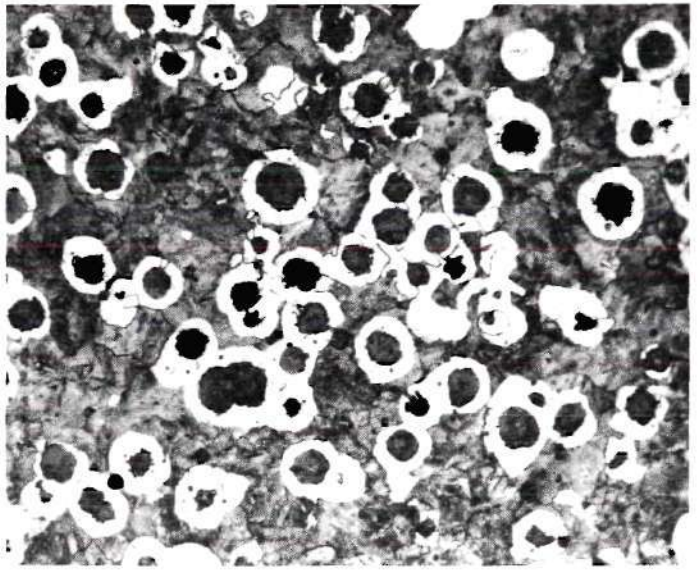

Figure 27(b) Alloy GT-58, 1/2 x 3/4 Inch Section, 2% Nital, x 200. (GT-58, C-3.70, Si-2.37, Mn-0.69, Mg-0.057).

isothermally held for 80 seconds and 130 minutes respectively at 1135°C.

Study of Nuclei of Graphite

Figure 28 shows the distributions of Si, Mn and C in specimen GT-41 quenched in water after 30 minutes. Scanning was performed across a graphite nodule embedded in quenched liquid (Figure 28(a)). The C, Si and Mn profiles do not show any segregation at the center of the graphite nodule. The distributions of C, Si and Mn in specimen isothermally held for 71 minutes also do not show any trace of the alloying elements at the center of the nodule.

In the present work, the microprobe scanning was performed across the nodules of several specimens of widely varying compositions, but none of the graphite nodules indicate any build up of solute concentration at the center. This result is in contrast to that obtained by Von Rosentiel and co-workers (72), who found a significant amount of Si at the center of the graphite nodule.

Study of the Matrix Structure

The distributions of C, Si and Mn surrounding the graphite nodule in unalloyed iron are shown in Figures 28(b) 28(c) and 28(d) which indicates the accumulation of C and Mn and depletion of Si in the quenched liquid. The variation in composition of the liquid is due to the partitioning of the alloying elements between the austenite and the cementite phase of the ledeburite eutectic.

Figure 29 illustrates the Si and Mn distribution as well as the microstructure of the same material isothermally held for 71 minutes at

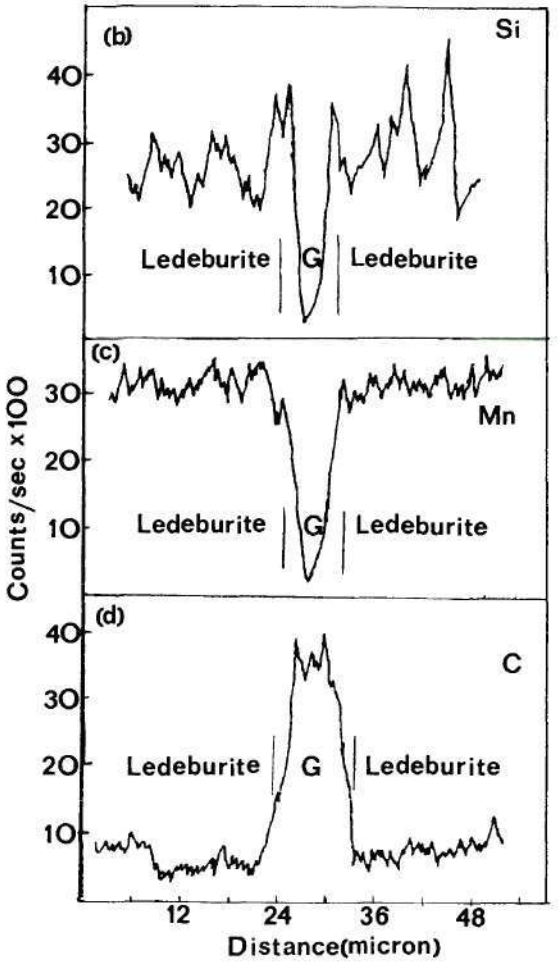

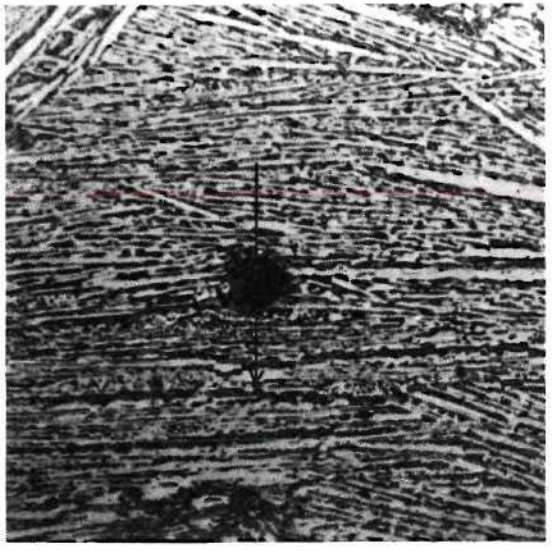

(a)

Figure 28. (a) Microstructure for Alloy GT-41 Quenched After Holding for 30 Minutes at 1128°C (b) Distribution of Si (c) Distribution of Mn (d) Distribution of C.

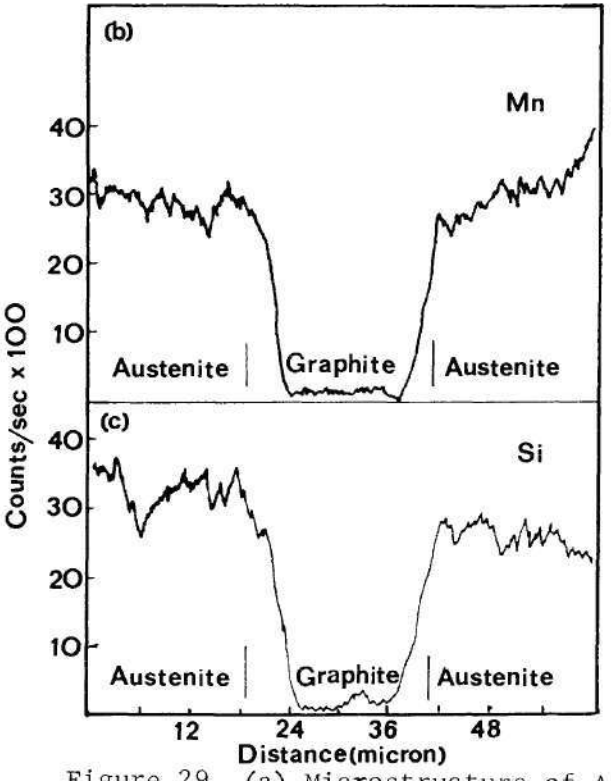

(a)

Figure 29. (a) Microstructure of Alloy GT-41 Quenched After Holding for 71 Minutes at 1128°C (b) Distribution of Mn (c) Distribution of Si.

1128°C. It is interesting to note that the concentration of Mn increases and Si decreases as the matrix is traversed away from the graphite nodule. Figure 30 demonstrates the concentration profiles for Si, Mn and Cu in alloyed iron across a graphite nodule surrounded by an austenite envelope and ledeburite eutectic in alloy GT-61. It can be seen from this figure that there is a sharp change in concentrations of Si, Mn and Cu at the austenite/ledeburite interface. Furthermore, Mn segregates in the quenched liquid (ledeburite eutectic) and Si and Cu are rejected from the liquid. The concentrations of Si and Cu were much lower in the liquid than in the austenite. These two elements tend to concentrate in the austenite phase of the ledeburite eutectic during solidification.

Figure 31 illustrates the microstructure and distributions of Si, Mn and Cu in the same material isothermally held for 130 minutes at 1130°C. It is evident from these graphs that the sharp change in concentration at the austenite/liquid (ledeburite) interface is completely eliminated. Due to the longer time of holding, cementite goes into solution in austenite and the carbon precipitates on the existing graphite spheroid. Thus the structure consists of graphite in a matrix of austenite of uniform composition.

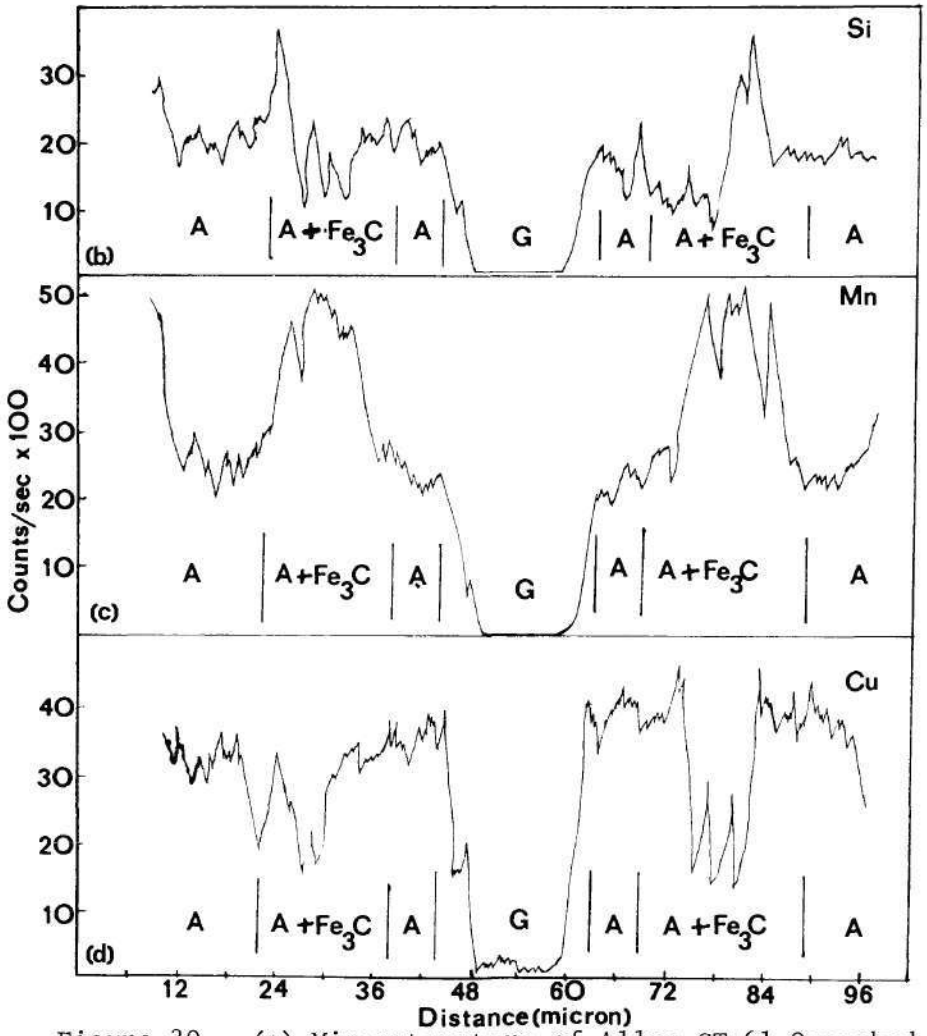

A-Austenite
G-Graphite
$A+Fe_3C$ → Ledeburite

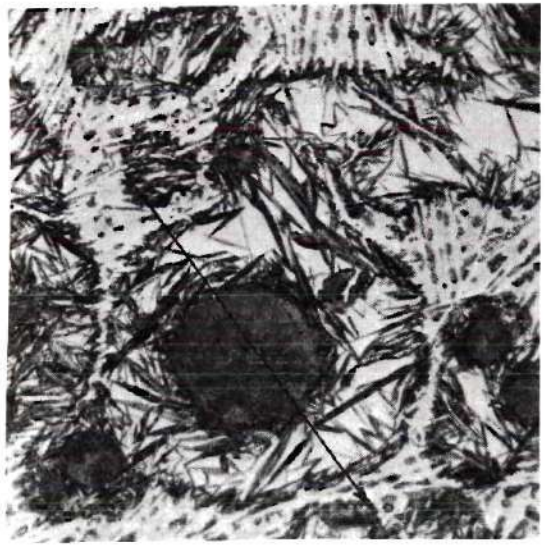

(a)

Figure 30. (a) Microstructure of Alloy GT-61 Quenched After Holding for 80 Seconds at 1130°C (b) Distribution of Si (c) Distribution of Mn (d) Distribution of Cu.

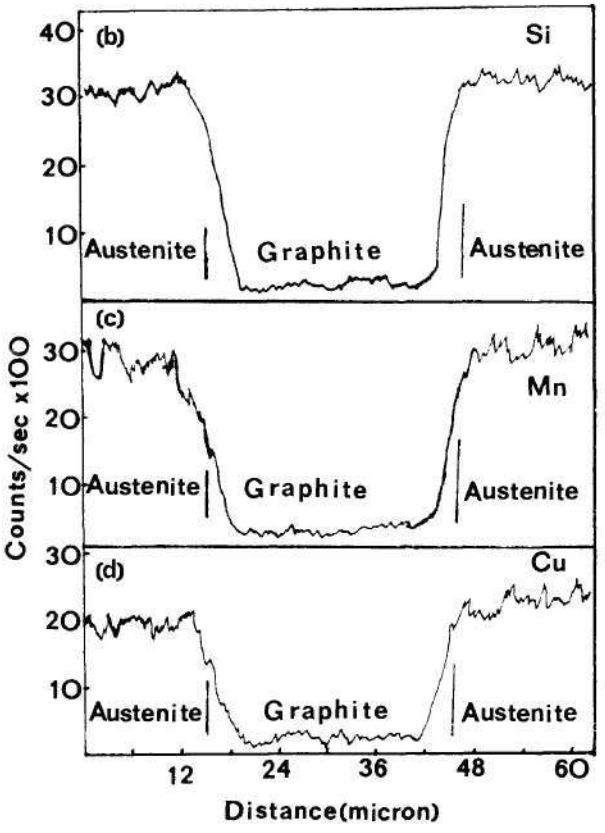

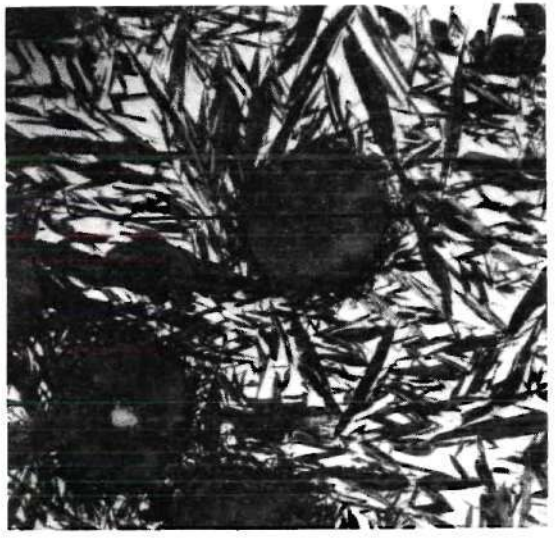

(a)

Figure 31. (a) Microstructure of Alloy GT-61 Quenched After Holding for 130 Minutes at 1130°C (b) Distribution of Si (c) Distribution of Mn (d) Distribution of Cu.

CHAPTER V

DISCUSSION OF RESULTS

Mechanism of Graphite Growth

Growth of graphite near the eutectic temperature occurs in three stages. In the first stage, the graphite grows in contact with the liquid during the process of solidification and in the second and third stage, the growth takes place in solid state. However, the growth in the first stage is not reflected in the isothermal curve which exhibits the second and third stages of growth. The sharp increase in the average size of the nodule and a rapid decrease in the nodule count (Figure 9) indicate that the isothermal growth of graphite at the second stage is attributable to the solution of cementite as well as the re-solution of smaller graphite nodules. In the third stage, the growth rate is very much retarded. The growth of graphite in this stage takes place due partly to the solution of residual carbide and partly to the solution of smaller nodules.

In fact, the rate of diffusion of carbon is very high at 1128°C but the driving force for dissociation of cementite is very low because of the lower degree of undercooling below the eutectic temperature. As a result the smaller nodules go into solution to maintain the equilibrium carbon content of austenite. From the standpoint of interfacial energy (58), it is clear that the surface energy per volume for the smaller nodules is greater. Consequently, the energy

of the system as a whole is reduced by the growth of the larger nodules at the expense of the smaller ones.

At lower temperature near 950°C, the size of the nodules also increases very rapidly at the beginning and then the nodule size remains essentially constant. This initial rapid growth rate followed by an almost zero growth rate can be explained by the T-T-T curve for decomposition of cementite. It has been found by the author that the decomposition of cementite is much faster at temperatures around 980°C than that at higher or lower temperatures. The curve depicted in Figure 9 is for an isothermal reaction at 950°C which is very close to the nose of the T-T-T curve. Therefore, the dissociation of cementite is still faster at 950°C than that at 1128°C.

In fact the rate of solution of cementite and diffusion of carbon atoms into the austenite are sufficient to maintain a constant carbon level in the austenite during the growth in the first stage, Whereas during the second stage the carbon replenishment from the cementite fails to keep pace with the depletion resulting from the growth of graphite, as a result re-solution of the smaller nodules takes place to maintain the constant carbon level in austenite. This mechanism can be further supported from the nucleation curve which shows a progressively reduction in nodule count with the increasing holding time at 950°C (Figure 9). The initial increase in nodule count is attributed to the growth of dormant spheroids which were not visible in the microstructure of the specimen quenched after 10 seconds.

Influence of Post-Inoculation

A comparison of the nucleation and the growth curves of post-inoculated iron with that of having no post-inoculation treatment clearly indicates that the number of graphite crystallization centers has been greatly increased by post-inoculation in an expected manner.

The initial small increase in nodule size within 45 seconds is primarily due to the rapid decomposition of cementite. Additionally, the re-solution of smaller nodules also contributes to the growth of graphite as is evident from the sharp drop in nodule count within a very short period (Figure 11). Since the major part of the eutectic cementite goes into solution at an earlier stage, the supply of carbon for the growth of graphite becomes very much restricted. As a result, the growth rate is very much retarded with longer holding time.

The mechanism of growth can be explained further with the aid of the micrographs presented in Figure 12. It can be seen that the structure of the specimen quenched after 13 seconds consists of large amounts of cementite at the positions between the austenite envelopes (Figure 12(d)). When the specimen is quenched after 45 seconds, most of the cementite is decomposed and the structure consists of graphite, austenite, martensite and a small trace of cementite (Figure 12(e)). Since the growth of graphite takes place by diffusion of carbon from cementite to the nodule via austenite envelope, the growth becomes very retarded when the major part of the cementite is decomposed. This is also reflected in the growth curve which shows that after 45 seconds the growth rate is very slow. With longer holding time the carbon

becomes uniformly distributed in the austenite and the structure contains uniformly distributed martensite. The growth of the nodule after 10,000 seconds is insignificant (Figure 12(f)) which is reflected in the growth curve.

Mechanism of Isothermal Decomposition of Cementite

It has been observed from the microstructurers of several specimens isothermally held at different temperatures that the molten iron when quenched down to the temperatures above the knee of the T-T-T curve exhibits the structure consisting of graphite, ledeburite and austenite. While quenching the melt to the temperatures below the knee of the T-T-T curve, the structure consists of secondary cementite in addition to graphite, ledeburite and austenite. The knee of the T-T-T curve for decomposition of cementite occurs in the temperature range 980^{o}C to 1080^{o}C depending on the composition.

The first stage graphitization above the nose of the T-T-T curve takes place by the solution of ledeburitic cementite in austenite and precipitation of carbon to the graphite. As a result the smaller spheroids grow in size with increasing holding time (Figures 14(a), 14(b), and 14(c)). The isothermal growth of graphite has been discussed previously and will not be elaborated here.

The presence of carbide in the quenched specimens indicates that a non-equilibrium cooling condition must exist during solidification (79) in order to facilitate the formation of carbides. During isothermal holding of the specimen just below the eutectic, the ledeburitic cementite dissolves and the structure approaches equilibrium with

respect to C, Si, Mn and other alloying elements. Similar conditions prevail during annealing of commercial ductile iron which contains residual carbides due to non-equilibrium solidification. The sequence of graphitizing reaction can be presented as follows:

Graphite + Ledeburite

→ Graphite + Austenite

When the molten iron is quenched down to the temperatures below the nose of the T-T-T curve, secondary cementite (6) appears in the structure with ledeburite and graphite as can be seen from the Figures 15(a) and 16(a). Cementite in the ledeburite dissociates during isothermal holding and the carbon diffuses to secondary cementite and graphite. When all the ledeburitic cementite is dissolved, the secondary cementite starts to go into solution in austenite and finally carbon precipitates on the graphite spheroids. The graphitizing reaction below the nose of the T-T-T curve is presented as follows:

Graphite + Ledeburite + Secondary Cementite

→ Graphite + Secondary Cementite + Austenite

→ Graphite + Austenite

The graphitizing reaction becomes more and more slugish when the holding temperature is increased above the nose of the T-T-T curve. The reason comes from the interplay between diffusion rate which increases with temperature and driving force which increases with undercooling below the melting point. The product of these two exhibits a maximum around the nose of the C curve where the breakdown of cementite

takes place in the shortest time.

Influence of Alloying Elements on T-T-T Curve

Influence of Si

Si is a strong graphitizer and increased addition of Si in cast iron lowers the residual carbide in the structure. It can be seen from Figure 17 that at temperatures near 980°C, the time for cementite dissociation is reduced from 58 to 38 seconds when Si is increased by about 2.0 per cent. By the same token, it can also be noted that at lower temperatures around 845°C, the time for cementite breakdown is reduced from 15,000 to 5,200 seconds. The influence of higher amount of Si on the speed of cementite dissociation reaction is more pronounced at the lower temperatures than that at the higher temperatures. This is mainly attributed to the increased driving force for decomposition of cementite at lower temperatures combined with the strong graphitizing potential of the alloy with higher amount of Si.

At higher temperatures, above the nose of the T-T-T curve, the free energy for decomposition of cementite approaches zero with increasing temperature. Consequently, the speed of cementite dissociation is not enhanced very much inspite of the higher diffusion rate of carbon at elevated temperature.

Influence of Mn

Manganese increases the stability of cementite by reducing the activity of carbon in the melt. Accordingly, the T-T-T curve for decomposition of cementite is shifted to the right when the Mn per cent is increased from 0.84 to 1.67. The T-T-T curve is moved further to the

right when the Mn is increased above 2.0 per cent (Figure 18). The effect of Mn on the matrix structure of alloys with 0.84 and 1.61 per cent Mn respectively (Heat GT-51 and 41) is shown on Figures 15(b) and 32. A close examination of these microstructures shows that for the alloy with 0.84 per cent Mn, the cementite dissociation reaction is over within 60 seconds at temperatures near the nose of the T-T-T curve. In contrast, the alloy with 1.6 per cent Mn, exhibits cementite and graphite after about the same holding time. It is also interesting to note that the alloy GT-41 (Table 1) has carbon equivalent 4.55 which is higher than the C.E. of alloy GT-51. Thus even with a higher C.E., the increased Mn per cent stabilizes the cementite during isothermal transformation.

Besides stabilizing the carbide in the matrix, Mn also stabilizes austenite as can be seen from the Figures 14(b) and 19. The amount of retained austenite in the specimen containing 1.62 per cent Mn is much higher than that with 0.84 per cent Mn.

Influence of Cr

Chromium is a strong carbide stabilizer and increases the ledeburitic eutectic temperature. At temperatures around 1040°C, the decomposition of cementite takes at least 400 seconds in the alloy with 0.38 per cent Cr. At the same temperature, it takes only 100 seconds to dissociate all cementite in the alloy with 0.04 per cent Cr (Figure 20). By comparison of the Figures 18 and 20, it is evident that the influence of Cr is much stronger than that of Mn in shifting the T-T-T curve. The nose of the T-T-T curve is raised to 1040°C with 0.38 per cent Cr whereas in the alloys with 0.04 per cent Cr, the nose

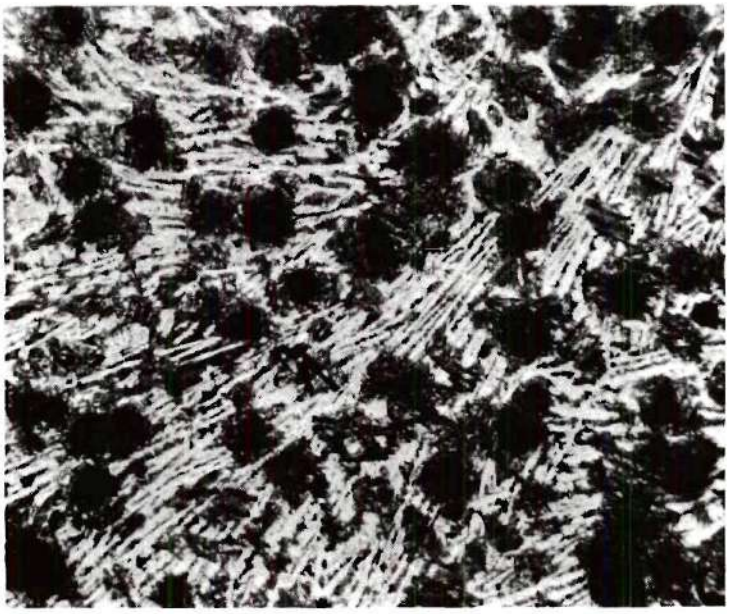

Figure 32. Alloy GT-41, 70 Seconds at 970°C, 2% Nital, x 200.

of the curve is around 980 to 1000°C. Since Cr raises the ledeburite eutectic temperatures of Fe-C equilibrium diagram (63), more than that of Mn, the maximum speed of dissociation of cementite is also moved to higher temperatures in the alloy with 0.38 per cent Cr.

Influence of Cu

According to the technical literature (68,69), Cu is a mild graphitizer and is insoluble in the graphite phase. Along the same line, Cu is not a carbide stabilizer and as such its solubility in cementite is expected to be negligible. Thus the physical properties of cementite reamin the same.

Results of the present investigation positively confirms that Cu is neither a strong graphitizer nor a carbide stabilizer. This is evident from Figure 21 which shows that the speed of cementite dissociation essentially remains unchanged even though the Cu content of the alloy is increased from .044 to 2.13 per cent. However, unlike Si and Mn, the speed of cementite decomposition of the alloys containing Cu is maximum at temperatures near 1080°C. Since Cu exerts a refining effect on the ledeburite eutectic, the effective surface area of the carbon rich crystal is increased and hence the solution of cementite in austenite takes place at a faster rate. As a result, the dissociation of cementite is completed much earlier at 1080°C than that around 980°C. Furthermore, Cu has an adverse influence (69) on the diffusion rate of carbon, thereby the decomposition of cementite at temperatures below 1080°C is progressively retarded even though the driving force is higher at lower temperatures.

Influence of Post-Inoculation on T-T-T Curve

The effects of post-inoculation have been studied by producing ductile iron heats in such a way that the final carbon equivalent of the melt is within 4.35-4.60. Thus the effect of different amounts of FeSi post-inoculant on the graphite morphology and matrix structure have been investigated at nearly equivalent compositions.

Figure 23 illustrates the influence of varying amounts of post-inoculant on the T-T-T curve for decomposition of cementite. There is a considerable increase in the speed of dissociation of cementite when the amount of post-inoculant is increased from 0.32 to 0.50 per cent. However, when the amount of post-inoculant is further increased to 1.0 per cent, the speed of cementite decomposition reaction is not significantly increased. This suggests that the optimum Si inoculation addition is reached around 0.50 per cent. Addition of larger amounts of FeSi is not advantageous. This result is in accord with that obtained by Shaw and Watmough (65) in their work on the effect of base silicon and post-inoculation on the microstructure of ductile iron.

The accelerated speed of cementite dissociation due to post-inoculation is evident from Figure 24 which shows a marked increase in nodule number for all section sizes. This enhancement in graphite crystalization centers lowers the diffusion distance for carbon atoms and thereby the graphitizing reaction is greatly increased.

Owing to the increased nodule number in post-inoculated iron, the volume of ferrite surrounding the graphite is also higher than that of the alloy in which Si addition is made prior to Mg treatment. The total volume of ferrite is also dependent on the section size of the

casting. This is mainly due to the reduction of cooling velocity which allows sufficient time for carbon atom to diffuse to the graphite and thus the area of the ferrite rim surrounding the nodule is greatly increased in higher section thickness.

When FeSi addition is made prior to Mg treatment, the nodule number does not increase significantly and consequently the diffusion path of carbon atom is considerably increased. As a result the transformation of austenite to ferrite is very much delayed causing more pearlite in the structure.

Since the number of graphite spheroids is much higher in thin sections due to faster cooling velocity, the pearlite content is relatively lower in thin section than that in thick sections as is evident from Figure 25.

Structural Correlation Between T-T-T Curve and Cooling Curve

Apart from shape, size, distribution of graphite spheroids, the mechanical properties of ductile iron also depend on the matrix structure. If the cooling curves for different section sizes are superimposed on the T-T-T curve for a particular composition of ductile iron, it is possible to establish a structure-section size relationship which can be used to predict the structure of ductile iron of a given composition.

In Figure 26, the cooling curve for 1/8 x 3/4 inch section does not cross the T-T-T curve for decomposition of cementite. This cooling curve is very steep, indicating rapid rate of cooling. Accordingly, solidification results in non-equilibrium condition. This gives rise

to residual carbide in the matrix as is evident from Figure 27(a). When the section size is increased to 1/2 x 3/4 inch, the solidification takes place at a slower rate and an equilibrium condition is closely approached. As a result if any cementite form, they are likely to dissociate, producing spheroidal graphite in the final structure. The cooling curve for 1/2 x 3/4 inch section cuts the T-T-T curve and the resulting structure is free from cementite (Figure 27(b)). This agreement between the cooling curves and the T-T-T curves can be used to predict the structure of ductile iron.

Identification of Graphite Nuclei

In the present study several graphite nodules were scanned with an electron beam of 1 micron diameter. It is evident from the concentration profiles for Si, Mn and Cu that these elements do not segregate at the center of the graphite nodule. Previous investigations by Von Rosentiel and co-workers (72) indicated that the presence of significant amount of Si at the center of the nodule in as cast ductile iron specimen. However, in this work ductile iron specimens isothermally treated near the eutectic freezing range were investigated.

According to the current theory, it is believed that the growth of graphite takes place by the diffusion of carbon towards graphite and simultaneous diffusion of Si and Fe away from the graphite to make room for its growth. Based on this hypothesis, it can be said that if Si or one of its compounds acts as the nucleating agent for graphite, then it should be present at the very beginning of the solidification process at the center of the nodule. However, no specimen quenched after a short

period showed any Si at the center of the nodule. Furthermore, the probability of hitting the center of the nodule is quite high since the depth of penetration of the electron beam in the graphite is approximately 3 microns (80) and it is most likely that out of several nodules with diameter ranging from 12 to 20 microns at least one nodule should be hit at the center. Therefore, it can be concluded that the presence of Si is not a prerequisite for heterogeneous nucleation of nodular graphite. However, it may act as nuclei under certain conditions, since Von Rosentiel and co-workers (72) identified the graphite nucleating agent as Magnesium-Silicon compound.

Distribution of Alloying Elements at Different Stages of Isothermal Transformations

It is well-known from the theories of binary alloy segregation that elements with an equilibrium distribution coefficient $K < 1$ should segregate at the solid/liquid interface as shown in Figure 5. The segregation patterns of C, Si and Mn indicate that Si is rejected at the austenite/ledeburite interface and Mn is absorbed by the liquid.

Furthermore, the irregular concentration profiles for Si and Mn indicate that Si concentrates in the austenite phase of the ledeburite eutectic. Mn, however, partitions both to the cementite as well as to the austenite phase from the liquid. The concentration of Mn in the cementite is a little higher than that of in austenite.

Since the affinity between carbon and Mn is very high, the presence of Mn in ledeburite retards the diffusion of carbon to the graphite and thus the cementite decomposition reaction is greatly slowed down

when higher amount of Mn is present in the ductile iron.

Si is a graphitizer and as such it tends to segregate in the austenite phase of the eutectic ledeburite. Because of the lower bonding energy between C and Si, cementite crystal always rejects Si into the austenite phase.

With prolonged isothermal holding, the cementite is completely dissolved and as a result the Mn and Si deficiencies are transferred to the austenite matrix. The Si and Mn concentration profiles of the specimen isothermally held for 71 minutes indicate that the concentration gradients of Mn is opposite to that of Si.

Alloyed Iron

Microanalytical results of the iron alloyed with 1.07 per cent Cu shows that the Si and Mn distributions are similar to that of unalloyed irons. However, Cu appears to form a solute rich layer at the austenite/ledeburite interface. Besides, the depletion of Cu in the ledeburite indicates that Cu is rejected at the freezing front during solidification.

Furthermore, unlike Mn, Cu has a tendency to concentrate in the austenite phase of the ledeburite eutectic. This clearly suggests that the bond energy between Cu and C is not very high and as a result Cu does not stabilize carbide.

The segregation of Cu in two phases of the ledeburite eutectic indicates that owing to the high temperature of the melt, the diffusion is likely to be very high and this faster diffusion rate allows partitioning of the alloying elements in the ledeburitic eutectic.

When the isothermal holding is prolonged, the irregularity in the distribution of Cu is completely eliminated and Cu becomes uniformly distributed in the austenite matrix as can be seen from Figure 31(d).

Mechanism of Solidification

The photomicrograph illustrated in Figure 28 shows a graphite nodule entrapped in the quenched liquid (ledeburite). Microprobe analyses for Si, Mn and C show that there is a build-up of Si at the graphite/melt interface. On the otherhand the concentration profile for C does not show any solute rich layer at the graphite melt interface. The absence of C segregation at the graphite/melt interface can be explained by the work of Hillert and Lange (31) who have shown mathematically that diffusion of carbon in liquid iron is 20 times greater than diffusion in solid austenite at the same temperature. Therefore the diffusion has obviously been sufficiently rapid to allow precipitation of carbon atoms on the graphite spheroid without leaving a carbon depleted zone. The presence of a Si rich zone at the graphite/melt interface indicates that the diffusion was not fast enough to allow Si atoms to move away from the growing edge of the graphite spheroid.

When an austenite envelop is present around the nodule the microanalytical results show that Si, Mn and Cu segregates at the solid austenite/liquid interface and Cu also segregates at the graphite/austenite interface, as can be seen from Figure 30.

Based on the microanalytical results from two different types of ductile iron structures (Figures 28 and 30), it is difficult to accept the current view (24) that graphite cannot grow without an

austenite-envelope. If an austenite envelope is always formed prior to quenching, the alloying elements would only segregate at the austenite/melt interface, and not at the graphite/melt interface. However, the results of the present work show that when the nodule is embedded in the melt, the solute atoms segregate at the graphite/melt interface. When there is a distinct growth of spheroid simultaneously with the austenite envelope, the solute segregates at the austenite/melt interface.

Therefore it can be concluded that the growth of spheroidal graphite takes place in two stages. At the first stage, the growth takes place in direct contact with the liquid and thus the solute atoms are rejected at the graphite/melt interface. In the second stage growth occurs in an envelope of austenite by diffusion of C toward the graphite and Fe, Si, Mn and other solute atoms away from the graphite (24). It is very difficult to accept that the growth occurs exclusively in an austenite envelope and not in direct contact with the melt.

In summation, the results of the present research can be applied to production processing. The T-T-T curve for decomposition of cementite would directly benefit in the planning of heat treatments of ductile iron. Due to the non-equilibrium nature of solidification, ductile iron is often susceptible to the formation of residual carbide in the cast structure. Presence of carbide in the structure lowers the machinability and ductility of the iron. This problem can be avoided if the casting is taken out of the mold in red hot condition and immediately charged into a furnace which is maintained at a temperature near the nose of the T-T-T curve. The cementite in the structure will be

decomposed within a short period and the casting need not have to be annealed for the removal of carbide. Thus there will be considerable saving in production time and cost.

The correlation between cooling curve and the T-T-T curve could be used to predict the structure of ductile iron of different section sizes. It would also be possible to estimate the mechanical properties of the iron from a quantitative measurement of ferrite, pearlite, carbide, nodule count and nodule size.

The present work yields information about the mechanism of growth of graphite during isothermal and athermal solidification of ductile iron. Isothermal growth of graphite takes place primarily by the solution of cementite at the very beginning and by the re-solution of smaller nodules at the later stage. Post-inoculation with FeSi accelerates the decomposition of cementite and thereby the growth of graphite is very much retarded.

During solidification under normal circumstances, the nucleation of graphite takes place in the liquid state. The initial growth of graphite occurs directly in contact with the liquid. At the later stage, the growth of graphite takes place within an austenite envelope. In the process of solidification, Si and Cu are rejected from the liquid and segregated into the austenite whereas Mn remains in solution and segregates in the cementite phase.

CHAPTER VI

CONCLUSIONS

The results of the present investigation can be summarized in the following conclusions:

1. Isothermal growth of graphite at an earlier stage is primarily controlled by the solution of cementite in austenite. Resolution of smaller nodules controls the growth of graphite at the later stage.

2. Post-inoculation with FeSi greatly enhances the nucleation rate of graphite and thereby the growth of graphite takes place at a faster rate.

3. The mechanism of isothermal graphitization above the nose of the T-T-T curve can be presented as:

$$\text{Graphite} + \text{Ledeburite} \rightarrow \text{Graphite} + \text{Austenite}$$

and that below the nose of the T-T-T curve can be summarized as:

$$\begin{aligned} &\text{Graphite} + \text{Ledeburite} + \text{Secondary Cementite} \\ \rightarrow\ &\text{Graphite} + \text{Secondary Cementite (Coarse)} + \text{Austenite} \\ \rightarrow\ &\text{Graphite} + \text{Austenite}. \end{aligned}$$

4. Addition of Si shifts the T-T-T curve for decomposition of cementite to shorter times. However, this effect is much stronger

when Si is added after magnesium treatment. This enhancement in the speed of cementite decomposition is attributed to an increase in the graphite nucleation centers and a decrease in the diffusion distance of carbon atoms.

5. Addition of 0.5 per cent FeSi as post-inoculant is found to be optimum when lower residual carbide, higher nodule count and good nodule distribution and nodule size are essential.

6. Cu does not have any significant influence on the speed of decomposition of cementite. However, unlike Si and Mn, Cu raises the nose of the T-T-T curve.

7. The correlation between cooling curves and the T-T-T curves enables one to predict the structure of ductile iron as a function of varying section sizes.

8. Formation of an austenite shell is not an essential condition for the growth of graphite spheroid during solidification process. The growth occurs directly in contact with the melt at an earlier stage of solidification.

9. Si and Cu segregate in the austenite phase and Mn segregates in the carbide phase in the process of solidification.

CHAPTER VII

RECOMMENDATIONS FOR FURTHER STUDIES

In the present investigation, the time-temperature-transformation curves for decomposition of cementite have been determined for ductile iron of varying compositions. Since the carbon content of austenite in cast iron is much higher than that of in steel, the T-T-T curve for decomposition of austenite would be a subject of further research. It would be very useful for the heat treatment of ductile iron.

Ni, Mo and Sn are added to ductile iron for improved strength properties. The influence of these elements on the T-T-T curve for decomposition of cementite should be investigated.

Small additions of Cu and Sn promotes pearlite in the ductile iron structure. The effect of Cu and Sn on the isothermal transformation of austenite should be studied in order to gain an understanding about the hardenability of ductile iron containing these elements.

One of the most important parts of this research was with the electron microprobe analyses of the graphite nodules. In order to get a deeper understanding about the nucleating agent of the spheroidal graphite, further investigation should be made on the graphite nodules separated from the iron. The electron diffraction pattern as well as the microprobe analyses of the isolated graphite would yield more information about the mechanism of nucleation of the spheroidal graphite in ductile iron.

APPENDIX I

MEASUREMENT OF FERRITE, PEARLITE AND CARBIDE BY POINT COUNTING SYSTEM

Point counting system involves counting the number of points of constituent phase in several fields of known size and calculating the per cent phase.

In the present study the ductile iron specimen was prepared by cutting sections at several random points and polishing and etching in 2 per cent nital to get a good contrast between ferrite, pearlite and carbide areas.

A standard Vickers Metallograph equipped with a 4" x 5" ground glass screen was used for point counting. Grid lines were scribed on a transparent plastic plate 1 cm apart, making a total of 24 of these line of intersections. Two such 25 points grids were drawn on the transparent plastic plate and used for counting at a magnification of 200. Every time a point is recorded when two grid lines intersect over an area of ferrite, pearlite or carbide. The per cent of each phase is determined by knowing the number of intersections falling over the desired phase area and the total number of line of intersections in the field.

In order to have a good representation, the sample was moved at random every time until a total of 80 fields were counted. Thus, each time 25 x 80 = 2000 points were counted for a particular specimen. The

per cent of each phase, the per cent probable error, mean value and standard deviation were calculated as follows:

$$\text{Percent Phase} = \frac{\text{Number of Phase Points}}{\text{Total number of Points}} \times 100$$

$$\text{Percent Probable Error} = \frac{\sqrt{\text{Fraction of Phase}}}{\sqrt{\text{Total Number of Points Counted}}} \times 100$$

$$\text{Mean } \bar{X} = \frac{\Sigma x}{N}$$

$$\text{Standard Deviation } (Sx) = \sqrt{\frac{\Sigma (x-\bar{x})^2}{N-1}}$$

Where N = Number of Observations

X = Individual values reported

ΣX = Sum of Individual Values

$\bar{X}$ = Mean of Values

Figure 33 shows a simulated photomicrograph with a grid screen superimposed over it. In this specimen, there are 37 points of pearlite and 5 points of ferrite in the matrix. Points falling at the interface between two phases are counted as 1/2. Therefore the per cents of pearlite and ferrite for this particular field are 74 and 10 respectively.

The accuracy of this system increases with the number of points counted as a square root ratio.

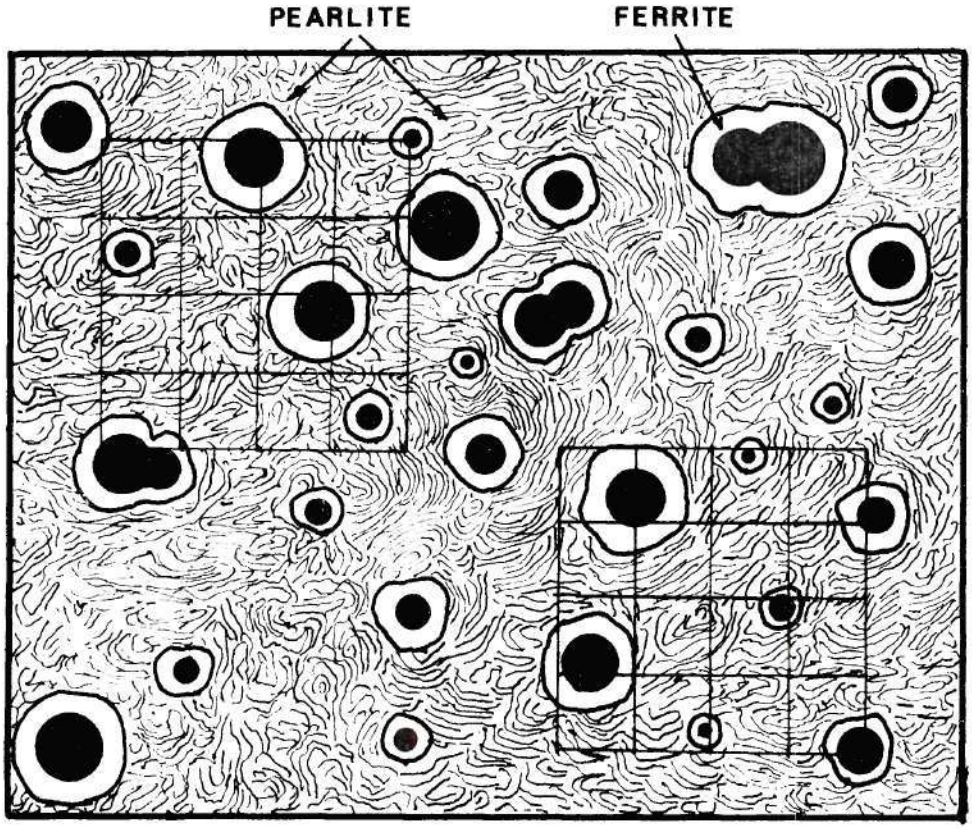

Figure 33. A Microstructure Showing Random Collection of Ferrite, and Pearlite Around the Graphite Spheroids.

Table 2. Mean Values, Standard Deviations and Per Cent Errors in the Measurement of Ferrite, Pearlite and Carbide Percentages for Heat GT-50 (C-3.70, Si-2.06, Mn-0.92 and Mg-0.045).

Phase	Section Size	Mean ($\bar{x}$)	Standard Deviation (Sx)	Percent Probable Error
Ferrite	1" x $\frac{3}{4}$"	5.300	2.6809	1.030
	$\frac{1}{2}$" x $\frac{3}{4}$"	5.796	2.7429	1.076
	$\frac{1}{4}$" x $\frac{3}{4}$"	4.006	2.3979	0.895
	$\frac{1}{8}$" x $\frac{3}{4}$"	0.525	0.9476	0.324
Pearlite	1" x $\frac{3}{4}$"	16.694	4.8146	1.827
	$\frac{1}{2}$" x $\frac{3}{4}$"	16.012	4.7554	1.790
	$\frac{1}{4}$" x $\frac{3}{4}$"	15.837	4.476	1.780
	$\frac{1}{8}$" x $\frac{3}{4}$"	12.619	4.0948	1.588
Carbide	1" x $\frac{3}{4}$"	-	-	-
	$\frac{1}{2}$" x $\frac{3}{4}$"	-	-	-

Table 2. (Continued)

Phase	Section Size	Mean ($\bar{x}$)	Standard Deviation (Sx)	Percent Probable Error
Carbide	$\frac{1}{4}$" x $\frac{3}{4}$"	2.356	1.9163	0.686
	$\frac{1}{8}$" x $\frac{3}{4}$"	9.637	4.1674	1.388

Table 3. Mean Values, Standard Deviations and Per Cent Errors in the Measurement of Ferrite, Pearlite, and Carbide Percentages for Heat GT-58 (C-3.70, Si-2.37, Mn-0.69 and Mg-0.057.

Phase	Section Size	Mean ($\bar{x}$)	Standard Deviation (Sx)	Percent Probable Error
Ferrite	1" x 3/4"	8.719	2.860	1.321
	1/2" x 3/4"	8.550	2.900	1.308
	1/4" x 3/4"	6.731	2.615	1.160
	1/8" x 3/4"	2.969	2.022	0.771
Pearlite	1" x 3/4"	12.637	3.766	1.590
	1/2" x 3/4"	13.050	3.731	1.616
	1/4" x 3/4"	15.350	4.476	1.752
	1/8" x 3/4"	17.006	5.322	1.844
Carbide	1" x 3/4"	-	-	-
	1/2" x 3/4"	-	-	-
	1/4" x 3/4"	-	-	-
	1/8" x 3/4"	2.031	3.610	0.637

Table 4. Coefficients for Schwartz-Saltykov Method of Calculating Particle Size Distributions.

	Coefficients, α_1						
j \ i→	$(N_A)_1$	$(N_A)_2$	$(N_A)_3$	$(N_A)_4$	$(N_A)_5$	$(N_A)_6$	$(N_A)_7$
$(N_v)_1$	+1.0000	0.1547	0.0360	0.0130	0.0061	0.0033	0.0020
$(N_v)_2$		+0.5774	0.1529	0.0420	0.0171	0.0087	0.0051
$(N_v)_3$			+0.4472	0.1382	0.0408	0.0178	0.0093
$(N_v)_4$				+0.3779	0.1260	0.0386	0.0174
$(N_v)_5$					+0.333	0.1161	0.0366
$(N_v)_6$						+0.3015	0.1081
$(N_v)_7$							+0.2773
N_v	+1.0000	+0.4227	+0.2583	+0.1847	+0.1433	+0.1170	+0.0988

Table 4. (Continued)

	Coefficients, α_1							
i→ / j	$(N_A)_8$	$(N_A)_9$	$(N_A)_{10}$	$(N_A)_{11}$	$(N_A)_{12}$	$(N_A)_{13}$	$(N_A)_{14}$	$(N_A)_{15}$
$(N_v)_1$	0.0013	0.0009	0.0006	0.0005	0.0004	0.0003	0.0002	0.0001
$(N_v)_2$	0.0031	0.0021	0.0015	0.0010	0.0009	0.0006	0.0006	0.0004
$(N_v)_3$	0.0057	0.0037	0.0026	0.0018	0.0013	0.0010	0.0007	0.0007
$(N_v)_4$	0.0095	0.0058	0.0038	0.0027	0.0020	0.0016	0.0012	0.0009
$(N_v)_5$	0.0168	0.0094	0.0059	0.0040	0.0028	0.0021	0.0016	0.0013
$(N_v)_6$	0.0346	0.0163	0.0091	0.0058	0.0041	0.0028	0.0022	0.0016
$(N_v)_7$	0.1016	0.0329	0.0155	0.0090	0.0057	0.0040	0.0029	0.0022
$(N_v)_8$	+0.2582	0.0961	0.0319	0.0151	0.0088	0.0056	0.0039	0.0028
$(N_v)_9$		+0.2425	0.0913	0.0301	0.0146	0.0085	0.0055	0.0039
$(N_v)_{10}$			+0.2294	0.0872	0.0290	0.0140	0.0083	0.0054
$(N_v)_{11}$				+0.2182	0.0836	0.0280	0.0136	0.0080
$(N_v)_{12}$					+0.2085	0.0804	0.0270	0.0132
$(N_v)_{13}$						+0.2000	0.0776	0.0261
$(N_v)_{14}$							+0.1925	0.0750
$(N_v)_{15}$								+0.1857
N_v	+0.0856	+0.0753	+0.0672	+0.0610	+0.0553	+0.0511	+0.0472	+0.0441

BIBLIOGRAPHY

1. K. D. Millis, Modern Casting, May, 1973, V. 63, No. 5, p. DI6.

2. K. P. Bunin and L. T. Kalinina, Dopovidi Akad. Nauk Ukr. R. S. R., 1231-5 (1960).

3. K. P. Bunin and N. G. Osada, Russian Castings Production, No. 6, p. 274-275, (1963).

4. Yu. V. Moiseev, G. A. Kutas and A. V. Chernovol, Russian Castings Production, p. 213-215, (1968).

5. C. D. D'Amico and R. Schneidewind, Transactions AFS, v. 48, p. 775, (1940).

6. A. P. Gagnebin, The Fundamentals of Iron and Steel Castings, The International Nickel Company, Inc., 4th Edition, (1968).

7. H. Morrough and W. J. Williams. Journal of the Iron and Steel Institute, v. 155, p. 321-271, (1947).

8. H. Morrough and W. J. Williams, Journal of the Iron and Steel Institute, v. 158, p. 306-322, March (1948).

9. R. P. Dunphy and W. S. Pellini, Foundry, v. 50, No. 1, p. 82-86, 195-196, 198-200, (1952).

10. B. Lux, AFS Cast Metals Research Journals, p. 25, v. 8, No. 1, p. 25, March (1972).

11. M. Hecht and J. C. Margarie, AFS Cast Metals Research Journal, p. 35, March (1973).

12. H. Siepman and F. W. Hanptvogel, Rheinstahl-Techn, V. 1,No. 1 ,p.16-23 (1963).

13. S. Banerjee, British Foundryman, v. 58, p. 344-353 (1965).

14. H. Kempers, Giesserei, p. 841-846, v. 53 (1966).

15. C. R. Loper and R. W. Heine, Transactions AFS, v. 72, p. 495, (1964).

16. E. Schiel and J. D. Schobel, Giesserei, techn-wiss. Beih, p. 203-213, v. 13 (1961).

17. J. D. Schobel, Recent Research in Cast Iron, Edited by H. D. Merchant, Gordon and Breach, p. 303 (1968).

18. E. Scheil, Giesserei, techn-wiss. Beih, p. 71-77, v. 14 (1962).

19. E. Scheil, Giesserei, techn-wiss. Beih., p. 1313-1338, No. 24, (1959).

20. H. Morrough, Journal of Iron and Steel Institute, v. 176, p. 378, (1954).

21. I. C. H. Hughes, Proc. Inst. Brit. Foundryman, v. 45, A157 (1952).

22. E. Scheil and L. Hutter, Arch. Eisenh, v. 24, p. 237 (1953).

23. H. Morrough, B.C.I.R.A. Journal of Research and Development, p. 655 v. 5, No. 12, June, 1955.

24. C. R. Loper and R. W. Heine, Trans. A.S.M. v. 56, p. 135 (1963).

25. G. Jolley and S. R. Holdsworth, Paper Presented at the Iron and Steel Institute's Annual Conference in Newcastle in June, 1971.

26. G. Jolley and J. A. Belk, B.C.I.R.A. Journal, v. 12, p. 651, (1964).

27. W. Oldfield, G. T. Geering and W. A. Tiller, The Solidification of Metals, Iron and Steel Institute Publication P. 110, p. 256-261, (1968).

28. B. Lux, AFS Cast Metals Research Journal, p. 162-164, v. 7, December (1971).

29. A. Riding and J. E. Gruzleski, Cast Metals Research Journal, v. 7, p. 162-164, December (1971).

30. G. Jolley, The Solidification of Metals, ISI P110, p. 242-250 (1968).

31. M. Hillert and N. Lange, J.I.S.I., v. 203, p. 273, 1965.

32. C. R. Loper and R. W. Heine, Transactions AFS, v. 69, p. 583 (1961).

33. R. P. Dunphy and W. S. Pellini, "Nodule Genesis and Growth in Magnesium Treated Hypoeutectie Irons", Memoires No. 8 Congress International de Fonderie, Brussels, (1951).

34. R. P. Dunphy and W. S. Pellini, Transactions AFS, v. 60, p. 775 (1952).

35. K. M. Htun, A.F.S. Cast Metals Research Journal, v. 6; p. 49, June (1970).

36. P.F. Wieser, C. E. Bates and J. F. Wallace, Mechanism of Graphite Formation in Iron-Silicon-Carbon Alloys, Malleable Founders Society, Cleveland, Ohio (1967).

37. C. R. Loper, Transactions AFS, v. 77, p. 1, (1969).

38. C. R. Loper and R. W. Heine, Grey Iron News, p. 4, June (1963).

39. S. I. Karsay, Transaction AFS, v. 73, p. 204 (1965).

40. A. DeSy, American Foundryman, v. 18, p. 55, (1949).

41. J. Keverian, H. F. Taylor and J. Wulf, American Foundryman, v. 22, p. 85, (1953).

42. M. Hamasumi, AFS Cast Metals Research Journal, v. 1, p. 9 (1965).

43. B. Lux, Recent Research on Cast Iron, Edited by H. D. Merchant, Gordon and Breach, p. 241 (1968).

44. B. Lux, Modern Castings, v. 45, p. 222, May (1964).

45. D. L. Sponseller, Thesis, University of Michigan (1962).

46. B. F. Brown and M. F. Hawkes, Transactions AFS, v. 59, p. 181 (1951).

47. W. A. Johnson, and R. F. Mehl, Trans. Amer. Inst. Min. Met. Eng., v. 135, p. 416-442, (1939).

48. M. C. Ashton and R. H. Newall, AFS Cast Metals Research Journal, v. 7, p. 18, March (1971).

49. J. Burke and W. S. Owen, Journal of Iron and Steel Institute, v. 176, p. 147, February (1954).

50. J. Burke and N. Swindells, ASM Seminar "Recent Research in Cast", Ed. H. D. Merchant, Gordon and Breach, (1968).

51. H. A. Schwartz, Symp. Graphitization of White Cast Iron, American Foundrymen's Association, v. 1 (1947).

52. A. Taub, Foundry, v. 86, p. 82, October (1958).

53. D. S. Gill and D. Epplesheimer, Foundry, v. 87, p. 60, August (1959).

54. B. Walker and V. Kondic, Journal of Iron and Steel Institute, v. 200, p. 1037 (1962).

55. Heine, Loper and Rosenthal, Principles of Metal Casting, American Foundrymen's Society, McGraw-Hill, p. 657.

56. J. Burke, Acta Met., v. 7 (1959).

57. C. E. Birchenall and H. W. Mead, J. Metals, v. 8, (1956).

58. W. S. Owen and J. Wilcock, Journal of Iron and Steel Institute, v. 182, p. 38, January (1956).

59. W. D. McMillan, Transactions AFS, v. 50, p. 30-38 (1942).

60. G. Sandoz, ASM Seminar "Recent Research on Cast Iron", Ed. H. D. Merchant, Gordon and Breach, p. 509, (1968).

61. J. Wilcock and J. Burke, ASM Seminar "Recent Research on Cast Iron", Ed. H. D. Merchant, Gordon and Breach, p. 551, (1968).

62. J. Pelleg, ASM Seminar, "Recent Research on Cast Iron", Ed. H. D. Merchant, Gordon andBreach, p. 573, (1968).

63. W. Oldfield, B.C.I.R.A. Journal, v. 10, No. 1, p. 17, January (1962).

64. J. W. Boyes, B.C.I.R.A. Journal, v. 9, No. 4, p. 499-505,July(1961).

65. W. F. Shaw and T. Watmough, Transactions AFS, v. 77, p. 380, (1969).

66. Strauss, Applied Science in the Casting of Metals, Pergammon Press, p. 181, (1970).

67. H. Morrough, B.C.I.R.A. Journal, v. 4. p. 292, (1954).

68. J. G. Pearce and K. Bromage, Copper in Cast Iron, C.D.A. publication No. 65, published by Hutchinson of London, p. 98, (1965).

69. A. DeSy, Transactions AFS v. 67, p. 321 (1959).

70. W. Oldfield, B.C.I.R.A. Journal, v. 9, p. 506-518, July (1961).

71. R. J. Warrick, AFS Cast Metals Research Journal, v.2, p. 98, September (1966).

72. A. P. Von Rosenstiel, H. Bakkerus and H. B. Zeedijk, AFS Cast Metals Research Journal, v. 2, March (1966).

73. A. L. DeSy, Metal Progress, p. 774, June (1950).

74. C. J. Peterson, Jr., Foundry, v. 101, p. 70, February (1973).

75. E. E. Underwood, Quantitative Sterology, Addison-Wesley, (1970).

76. R. T. DeHoff and F. N. Rhines, Quantitative Microscopy, McGraw-Hill, p. 149, (1968).

77. S. Epstein, The Alloys of Iron and Carbon, v. 1, p. 263, McGraw-Hill, New York, (1936).

78. H. S. Rawdon and S. Epstein, Bur. Stand. Sci. Paper 452, v. 18, p. 373-410, 1922-1923.

79. K. R. Olen and R. W. Heine, Transaction AFS, v. 76, p. 369 (1968).

80. James Johnson, Private Communication, Engineering Experiment Station, Georgia Institute of Technology, Atlanta, Georgia.

VITA

Nirmal K. Datta was born in Calcutta, India on April 14, 1945. There he attended public schools and graduated from the Serampore Union Institution in 1962. He entered the University of Calcutta in August, 1962 and was awarded a Bachelor's degree in Metallurgical Engineering in August, 1967. In the same year, he enrolled at the Indian Institute of Technology and received his Master of Technology degree in Foundry Engineering in August, 1969.

He came to United States in September, 1969 and was admitted to the School of Chemical Engineering at the Georgia Institute of Technology. He did his M.S in Metallurgy in June, 1971.

While at Georgia Tech, he presented a paper at the 49th general meeting of the Ductile Iron Society and co-authored a paper entitled 'Annealing Characteristics of Triple E Electrical Conductor Alloy' which will shortly appear in the Wire Journal. During his studies at Georgia Tech, he was awarded the Atlantic Steel fellowship and the Ductile Iron Society fellowship.

He is a member of American Foundrymen's Society, American Society for Metals and American Institute of Mining, Metallurgical and Petroleum Engineers and the Indian Institute of Metals.